The Astronomical Journal, 158:187 (21pp), 2019 November https://doi.org/10.3847/1538-3881/ab4130

Constraints on the Occurrence and Distribution of 1–20 $M_{\rm Jup}$ Companions to Stars at Separations of 5–5000 au from a Compilation of Direct Imaging Surveys

Frédérique Baron[1], David Lafrenière[1], Étienne Artigau[1], Jonathan Gagné[1], Julien Rameau[1,2], Philippe Delorme[2], and Marie-Eve Naud[1]
[1] Institut de Recherche sur les Exoplanètes, Département de Physique, Université de Montréal, Montréal, QC H3C 3J7, Canada
[2] Université de Grenoble Alpes, CNRS, IPAG, F-38000 Grenoble, France
Received 2019 January 15; revised 2019 August 23; accepted 2019 August 28; published 2019 October 17

Abstract

We present the first statistical analysis of exoplanet direct imaging surveys combining adaptive optics (AO) imaging at small separations with deep seeing-limited observations at large separations allowing us to study the entire orbital separation domain from 5 to 5000 au simultaneously. Our sample of 344 stars includes only confirmed members of nearby young associations and is based on all AO direct-imaging detection limits readily available online, with addition of our own previous seeing-limited surveys. Assuming that the companion distribution in mass and a semimajor axis follows a power-law distribution and adding a dependence on the mass of the host star, such as $d^2n \propto fM^{\alpha}a^{\beta}(M_{\star}/M_{\odot})^{\gamma}dMda$, we constrain the parameters to obtain $\alpha = -0.18^{+0.77}_{-0.65}$, $\beta = -1.43^{+0.23}_{-0.24}$, and $\gamma = 0.62^{+0.56}_{-0.50}$ at a 68% confidence level, and we obtain $f = 0.11^{+0.11}_{-0.05}$ for the overall planet occurrence rate for companions with masses between 1 and 20 $M_{\rm Jup}$ in the range of 5–5000 au. Thus, we find that occurrence of companions is negatively correlated with a semimajor axis and companion mass (marginally) but is positively correlated with the stellar host mass. Our inferred mass distribution is in good agreement with other distributions found previously from direct imaging surveys for planets and brown dwarfs, but is shallower as a function of mass than the distributions inferred by radial velocity surveys of gas giants in the 1–3 au range. This may suggest that planets at these wide and very wide separations represent the low-mass tail of the brown dwarfs and stellar companion distribution rather than an extension of the distribution of the inner planets.

Unified Astronomy Thesaurus concepts: Exoplanets (498); Direct imaging (387); Brown dwarfs (185)

Supporting material: machine-readable table

1. Introduction

Over the last 15 years, many teams—using several telescopes on the ground and in space—surveyed young nearby stars to uncover new planets with direct imaging (Lafrenière et al. 2007; Marois et al. 2008; Delorme et al. 2013b; Macintosh et al. 2015; Naud et al. 2017). All in all, about 1000 unique stars were observed in the search of planets using first-generation adaptive optics (AO) systems, seeing-limited imaging, or space-based telescopes. The orbital separations probed by these surveys range from several astronomical units to hundreds and even thousands of astronomical units, while the detectable planet masses are restricted to that of Jupiter or higher. Some of these surveys targeted only higher mass stars (Vigan et al. 2012; Nielsen et al. 2013; Rameau et al. 2013b), others aimed only at low-mass stars (Bowler et al. 2015; Galicher et al. 2016; Lannier et al. 2016; Naud et al. 2017), and some surveyed stars of all spectral types (Lafrenière et al. 2007; Heinze et al. 2010a; Biller et al. 2013; Chauvin et al. 2015; Meshkat et al. 2017; Uyama et al. 2017; Baron et al. 2018; Stone et al. 2018). Although only a few planets have been found through these efforts, the resulting large data set can be used to investigate the occurrence rate and distribution of planets as well as their dependence on the star properties. Such studies are necessary to gain knowledge about the formation and evolution of planets at the large orbital separations probed by direct imaging. This is particularly important since the standard planet formation models—core accretion or disk instability—struggle to form planets beyond 100 au.

One of the first attempts to constrain the orbital separation distribution and the mass distribution of Jupiter-like planets was made by Tabachnik & Tremaine (2002). Using data on 72 planets found by radial velocity (RV) and a distribution such as $dn = C(M)^{-\alpha}(P)^{-\beta}d\ln M d\ln P$, where M is the planet mass and P the orbital period, they inferred that $\alpha = 0.11 \pm 0.10$ and $\beta = -0.27 \pm 0.06$ for $M \lesssim 10\,M_{\rm Jup}$ and 2 days $< P <$ 10 yr. This idea was then pushed further by Cumming et al. (2008) who also used a power law to fit the distribution of planets with masses over 0.3 $M_{\rm Jup}$ and periods less than 2000 days detected using RV measurements of FGK stars. With a mass-period distribution of $d^2n = C(M)^{\alpha}(P)^{\beta}d\ln M d\ln P$, they obtained a constraint on the parameters of $\alpha = -0.31 \pm 0.20$ and $\beta = 0.26 \pm 0.10$. Also based on RV measurements of 166 stars, Howard et al. (2010) found that planet occurrence increases with decreasing planet mass, such as $dn = 0.39M^{-0.48}d\ln M$. Dong & Zhu (2013) studied *Kepler* planets with $P < 250$ days and found that the distribution of planets in terms of periods, $dn/d\ln P$, is proportional to $P^{0.7\pm0.1}$ for a Neptune-sized planet and agrees with a flat distribution for super-Earth or Earth-sized planets. Fernandes et al. (2019), based on transit and RV data, described the distribution of giant planets as a broken power law in a semimajor axis, showing initially an increase of planet occurrence with a semimajor axis, a turnover at about 3 au, followed by a decrease. They also found a power-law distribution in planet mass, showing an increase in occurrence for lower masses. All of those studies mostly focus on close-in planets of various masses, and there are very few constraints on semimajor axes greater than 10 au and even fewer over 100 au. However, the distribution of planets as presented in Cumming et al. (2008) was widely used, and still is, when planning surveys with direct imaging, as a way to predict the planet yield of the survey.

Table 1
Young Moving Groups

Name	Short Name	Distance	Age (Myr)	References
β Pictoris	BPIC	9–73	24 ± 3	Shkolnik et al. (2017)
AB Doradus	ABD	37–77	149^{+51}_{-19}	Bell et al. (2016)
Argus	ARG	29-118	40–50	Torres et al. (2008), Zuckerman (2019)
Carina	CAR	46–88	45^{+11}_{-7}	Bell et al. (2016)
Columba	COL	35–81	42^{+6}_{-4}	Bell et al. (2016)
Tucana–Horologium	THA	36–71	45 ± 3	Bell et al. (2016)
TW Hya	TW	8–92	10 ± 3	Bell et al. (2016)
Hercules-Lyra	HLY	~30	260±50	Eisenbeiss et al. (2013)
Lower Centaurus Crux	LCC	~140	16 ± 2	Pecaut & Mamajek (2016)
ϵ Chamaeleontis	EPSC	~100	3.7 ± 4.6	Murphy & Lawson (2015)
Upper Scorpius	US	~130	10 ± 2	Pecaut & Mamajek (2016)
Octans	OCT	~130	35 ± 5	Murphy et al. (2013)
Carina-Near	CN	~30	~200	Zuckerman et al. (2006)

Constraining the planet distribution of massive planets on wide orbits is needed to get more accurate planet yields.

A few constraints on the planet distribution do exist for separations beyond 10 au from direct imaging data. For instance, Heinze et al. (2010a) used their AO planet imaging survey to rule out with 90% confidence a distribution as in Cumming et al. (2008) at separations up to 110 au. Brandt et al. (2014) used a combined sample of direct imaging data to model the population of companion with masses 5–70 $M_{\rm Jup}$ and semimajor axes of 10–100 au with a power law. They found that $dn \propto M^{-0.65\pm0.60}a^{-0.85\pm0.39}$, which does not agree with the distribution of planets from Cumming et al. (2008) and hints that the low-mass companions in their sample represent the low-mass tail of the brown dwarf distribution. Reggiani et al. (2016) showed that the results from direct imaging surveys searching for substellar companions around Sun-like stars are consistent with an extrapolation of the Cumming et al. (2008) distribution to larger separations combined with the log-normal brown dwarf mass distribution from Raghavan et al. (2010). Lastly, Meyer et al. (2018) studied planets with masses between 1 and 10 $M_{\rm Jup}$ and separations between 0.07 and 400 au and found that the semimajor axis distribution is best described by a log-normal distribution peaking at about 3 au. For larger separations, there are virtually no constraints to date.

In this work, we merged different direct imaging surveys to constrain the occurrence rate and distribution of companions with masses between 1 and 20 $M_{\rm Jup}$ at orbital separations of 5–5000 au. Section 2 describes the sample of stars and observations taken from the Direct Imaging Virtual Archive (DIVA) and some other previous surveys made by our team. In Section 3, we first establish a planet detection completeness map for each target in our sample, and then use those to determine the occurrence rate of companions and, through a Markov chain Monte Carlo (MCMC) approach, constrain the parameters governing their distributions. We discuss our results and their implications in Section 4 and conclude in Section 5.

2. Sample

We assembled a sample of stars that were observed by AO direct-imaging planet searches, as well as by the seeing-limited PSYM-WIDE (Naud et al. 2017) and WEIRD (Baron et al. 2018) surveys. We focused on the stars that are confirmed members of young moving groups with ages of less than 300 Myr, meaning that they have a RV measurement, a trigonometric parallax, and *XYZUVW* values consistent with the moving group spatial's position and space velocity, as well as independent signatures of youth, such as spectroscopic signs of low-gravity, strong X-ray or UV emission, or lithium absorption. Table 1 presents the young moving groups to which our stars belong, namely TW Hya (de la Reza et al. 1989; Kastner et al. 1997), β Pictoris (Zuckerman et al. 2001a), AB Doradus (Zuckerman et al. 2004), Tucana–Horologium (Torres et al. 2000; Zuckerman et al. 2001b), Carina (Torres et al. 2008), Columba (Torres et al. 2008), Argus (Makarov & Urban 2000), Carina-Near (Zuckerman et al. 2006), Upper Scorpius (USCO; Pecaut & Mamajek 2016), Lower Centaurus Crux (LCC; Pecaut & Mamajek 2016), ϵ Chamaeleontis (Murphy et al. 2013), Hercules-Lyra (Eisenbeiss et al. 2013), or Octans (Murphy et al. 2013). We have included the star that is a member of Hercules-Lyra, even if Mamajek (2016) indicated that Hercules-Lyra might be a stream and not a real association.

The WEIRD survey (Baron et al. 2018) surveyed 177 stars of all spectral types using deep seeing-limited imaging to search for giants planets on very wide orbits. A typical completeness of 2 $M_{\rm Jup}$ is reached, while some stars of the younger/nearer groups have a 1 $M_{\rm Jup}$ detection limit, at separations between 1000 and 5000 au. We added all the objects from the WEIRD survey in our sample, as they are all bona fide members of young associations.

The PSYM-WIDE survey (Naud et al. 2017) observed 95 M dwarfs using seeing-limited imaging, out of which only 10 were bona fide members of nearby young moving groups, the others being nonconfirmed candidate members at the time of publication. However, using the *Gaia* DR2 release (Gaia Collaboration et al. 2018; Lindegren et al. 2018) and the web tool BANYAN Σ from Gagné et al. (2018), we confirmed the membership of 34 stars out of those 85 candidates; see Table 2. The total number of bona fide members from PSYM-WIDE used in our study is thus 44. The survey reached good completeness for a mass of 10 $M_{\rm Jup}$ or more at semimajor axes larger than 1000 au.

To complement the above seeing-limited observations, sensitive to the widest orbital separations, we used the DIVA archive (Vigan et al. 2017) to extract data for 119 stars that are bona fide members of young associations of less than 300 Myr and that were observed at closer separations by Masciadri et al. (2005),

Table 2
Confirmed Members from PSYM-WIDE

2MASS Name	R.A. (J2000.0)	Decl. (J2000.0)	Probability %	Association
J00325584−4405058	8.2326770	−44.084965	99.3	ABD
J00374306−5846229	9.4294440	−58.773033	99.7	THA
J01123504+1703557	18.146006	17.065475	99.1	ABD
J01521830−5950168	28.076262	−59.838001	>99.9	THA
J02045317−5346162	31.221569	−53.771183	>99.9	THA
J02070176−4406380	31.758289	−44.112339	>99.9	THA
J02215494−5412054	35.478949	−54.201511	>99.9	THA
J02224418−6022476	35.684107	−60.379906	80.0	CAR
J02340093−6442068	38.503875	−64.701912	>99.9	THA
J02485260−3404246	42.219191	−34.073517	99.8	COL
J02564708−6343027	44.196205	−63.717438	90.4	CAR
J03350208+2342356	53.758697	23.709892	99.0	BPIC
J04091413−4008019	62.308892	−40.133862	>99.9	COL
J04213904−7233562	65.412690	−72.565613	>99.9	THA
J04363294−7851021	69.137280	−78.850594	96.0	ABD
J04402325−0530082	70.096891	−5.5022970	96.4	CN
J04440099−6624036	71.004021	−66.402084	97.1	THA
J04571728−0621564	74.322039	−6.3656870	99.8	ABD
J05241317−2104427	81.054884	−21.078550	>99.9	COL
J05335981−0221325	83.499224	−2.3590290	>99.9	BPIC
J05395494−1307598	84.978924	−13.133292	95.4	COL
J06112997−7213388	92.874897	−72.227448	94.8	CAR
J08173943−8243298	124.41432	−82.724945	99.7	BPIC
J12383713−2703348	189.65473	−27.059681	99.7	ABD
J18420694−5554254	280.52895	−55.907082	99.8	BPIC
J19560294−3207186	299.01626	−32.127125	93.5	BPIC
J20004841−7523070	300.20174	−75.385284	99.8	BPIC
J21100535−1919573	317.52232	−19.332603	99.8	BPIC
J22021626−4210329	330.56775	−42.175831	99.4	THA
J23131671−4933154	348.31962	−49.554298	>99.9	THA
J23285763−6802338	352.24016	−68.042747	98.6	THA
J23320018−3917368	353.00077	−39.293564	>99.9	ABD
J23452225−7126505	356.34272	−71.447380	>99.9	THA
J23474694−6517249	356.94561	−65.290260	>99.9	THA

Biller et al. (2007), Lafrenière et al. (2007), Kasper et al. (2007), Chauvin et al. (2010), Heinze et al. (2010a), Vigan et al. (2012), Rameau et al. (2013b), Chauvin et al. (2015), Meshkat et al. (2015a), or Meshkat et al. (2015b). Out of the 119 stars, 73 have also been observed by the WEIRD or the PSYM-WIDE surveys at larger separations. Overall, the completeness maps of these targets reach good completeness at 3 $M_{\rm Jup}$ over a range of semimajor axes of 50–5000 au.

We also used data from the AO survey of Upper Scorpius stars of Lafrenière et al. (2014). They list 91 stellar members of Upper Scorpius, and 84 of them have a parallax in *Gaia* DR2. One of them, HIP 78265, was rejected from our sample because its new *Gaia* parallax puts it at a distance of 590 pc, which is too far from the other members of Upper Scorpius. All other stars with parallaxes from that study were kept. This survey probes an intermediate range of semimajor axes compared to the above AO imaging survey, with a good completeness between 200 and 800 au for companions with masses as low as 10 $M_{\rm Jup}$, as the members of this association are further away than most of the other targets in the sample.

Table 3 lists the 344 unique stars in our sample, along with their R.A., decl., spectral type, proper motion in R.A. and decl., association, and distance. Figure 1 presents the summary of our sample. The median target has a distance of 50 pc, a proper motion of 80 mas yr^{-1}, and an age of 24 Myr. The spectral types of the targets range from B to L dwarfs, and most of the targets are M dwarfs.

Seven stars in our sample are known hosts of companions ($M < 20\,M_{\rm Jup}$) on wide orbits : 51 Eri, HR 8799, β Pictoris, AB Pic, Gu Psc, TWA 27, and 1RXS J160929.1-210524. Each system is described briefly below.

1. 51 Eri b is a 2–10 $M_{\rm Jup}$ planet orbiting the F0IV star 51 Eri at a projected separation of ∼14 au; it was found with the Gemini Planet Imager (GPI) at Gemini (Macintosh et al. 2015). While the star is part of our sample, the companion was not detected in the data we compiled.
2. HR 8799 hosts four planets of 7^{+4}_{-2}, 10 ± 3, 10 ± 3 and 9 ± 4 $M_{\rm Jup}$ (Marois et al. 2008, 2010) at semimajor axes of, respectively, $70^{+0.19}_{-0.18}$, $43.1^{+1.3}_{-1.4}$, $26.2^{+0.9}_{-0.7}$, and 16.2 ± 0.5 au, assuming stable coplanar orbits (Wang et al. 2018). Rameau et al. (2013b), whose data are part of our study, were able to recover planets (b), (c), and (d), but not planet e due to the small parallactic angle rotation of the observation. We assume in this work that HR 8799 is an A5V star member of the Columba association, although its membership has been questioned. However, signs of youth are present in the planets' spectra and

Table 3
Properties of the Sample of Bona Fide Members

Name	R.A. (J2000.0)	Decl. (J2000.0)	SpT	$\mu_\alpha \cos\delta$ (mas yr^{-1})	μ_δ (mas yr^{-1})	Association	Distance (pc)	Masses ($M_\odot$)	Surveys
HIP 490	00 05 52.54	−41 45 11.0	G0V	97.53 ± 0.38	−76.27 ± 0.44	THA	39.385 ± 0.915	1.53	3
HD 203	00 06 50.08	−23 06 27.1	F2IV	96.77 ± 0.13	−47.12 ± 0.06	BPIC	39.960 ± 0.099	1.33	3
HIP 1113	00 13 53.01	−74 41 17.8	G8V	83.53 ± 0.78	−47.89 ± 0.75	THA	44.404 ± 1.616	1.18	3
HD 984	00 14 10.25	−07 11 56.8	F5V	104.53 ± 0.15	−67.91 ± 0.06	COL	45.911 ± 0.118	1.00	3
2MASS J00172353-6645124	00 17 23.53	−66 45 12.4	M2.5	102.90 ± 1.00	−15.00 ± 1.00	ABD	51.241 ± 0.120	1.56	10

References. (1) Biller et al. (2007), (2) Chauvin et al. (2010), (3) Chauvin et al. (2015), (4) Heinze et al. (2010a), (5) Kasper et al. (2007), (6) Lafrenière et al. (2007), (7) Masciadri et al. (2005), (8) Meshkat et al. (2015a), (9) Meshkat et al. (2015b), (10) Rameau et al. (2013b), (11) Vigan et al. (2012), (12) Naud et al. (2017), (13) Lafrenière et al. (2014), (14) Baron et al. (2018).

(This table is available in its entirety in machine-readable form.)

Zuckerman et al. (2011) have shown that HR 8799 is younger than the Pleiades.

3. β Pictoris, an A6V star member of the β Pictoris moving group, hosts a $11 \pm 2\,M_{\rm Jup}$ planet (Lagrange et al. 2009; Snellen & Brown 2018) with a semimajor axis of $9.2^{+1.5}_{-0.4}$ au (Millar-Blanchaer et al. 2015). Rameau et al. (2013b) were also able to recover this companion.
4. AB Pic b is a $13.5 \pm 0.5\,M_{\rm Jup}$ object at a projected separation of 250 au from AB Pic, a K2V star member of the Tucana–Horologium association (Chauvin et al. 2005). It was recovered by Rameau et al. (2013a) and also tentatively recovered by Biller et al. (2007).
5. GU Psc, an M3V star member of the AB Doradus association, is host to a $11 \pm 2\,M_{\rm Jup}$ companion (Naud et al. 2014) at an angular separation of 42″. We used the new parallax from *Gaia* DR2 to revise the projected separation estimate to 1998 ± 6 au. The discovery observations were part of the PSYM-WIDE survey.
6. TWA 27 hosts a $4 \pm 1\,M_{\rm Jup}$ companion (Chauvin et al. 2004) at a projected separation of 46^{+37}_{-15} au (Blunt et al. 2017). The host is a young brown dwarf, member of the TW Hydrae association at 52 pc. The planet was discovered using the Very Large Telescope (VLT) with the NACO instrument but it was not detected in the images used in our survey.
7. As part of the Upper Scorpius survey used in the present study, Lafrenière et al. (2008, 2010) found a directly imaged planet around 1RXS J160929.1-210524, an M0 star member of the Upper Scorpius association. 1RXS J160929.1-210524b has a mass between 7 and 12 $M_{\rm Jup}$ (Lachapelle et al. 2015) and a projected separation of 320 ± 40 au.

The sample of our study thus includes five detected planet-hosting stars and seven detected planets. Four of those orbit BA stars, two orbit FGK stars, and one is around an M dwarf. The small number of planets around M dwarfs in our sample may seem surprising, given the large number of M dwarfs in our sample and the relatively large number of companions found by direct imaging around M dwarfs (e.g., Rebolo et al. 1998; Itoh et al. 2005; Luhman et al. 2006, 2009; Reid & Walkowicz 2006; Goldman et al. 2010; Todorov et al. 2010; Ireland et al. 2011; Bowler et al. 2013; Delorme et al. 2013a; Kraus et al. 2014; Naud et al. 2014; Artigau et al. 2015; Gauza et al. 2015; Deacon et al. 2016; Dupuy et al. 2018), but we point out that out of all those detections only two were found around M bona fide members of young associations (Chauvin et al. 2004; Naud et al. 2017).

3. Analysis

We used the 7σ detection limits as a function of angular separation provided by the DIVA archive, by Baron et al. (2018), by Naud et al. (2017), and by Lafrenière et al. (2014) to build the completeness maps for each target. We first defined a 100×100 grid of masses and semimajor axes, with the masses equally spaced in logarithmic scale between 1 and $20\,M_{\rm Jup}$ and the semimajor axes equally spaced in logarithmic scale between 5 and 5000 au. At each point of the grid, 10^4 planets were simulated, each having an eccentricity taken randomly from the beta function eccentricity distribution reported in Kipping (2013), which is taken from the eccentricity distribution of RV planets as well as a random inclination and orbital phase, which then yield a projected separation for each planet. Following the method described in Baron et al. (2018) and using the AMES.Cond evolution models (Allard et al. 2001; Baraffe et al. 2003) to convert the planets masses to flux, we compared the planet's magnitudes to the detection limits found earlier to assess the detectability of each planet. If the detection limits were provided in planet-to-star contrast, they were converted into the detection limit in the planet absolute magnitude using the star's magnitudes. We then obtained completeness maps for all of the stars in the sample. If a given star was observed by two or more surveys, the most sensitive detection probability was adopted at each point of the mass–separation grid, and we assumed that the exoplanet did not move on its orbit between the different observations. As some of the calculations that follow will need it, a similar completeness map was calculated for each star but this time directly over a grid of projected separations instead of semimajor axes. For this latter approach, there was no need to draw orbital parameters randomly as the fiducial planets were directly generated at projected separations that can be compared directly with the detection limits.

At 5000 au, about half of the stars in the sample have a $> 60\%$ probability of detecting a companion of mass anywhere in the range of 1–20 $M_{\rm Jup}$, while about 20% of the stars have this same probability at 20 au, and 10% at 5 au. We choose a lower mass limit of $1\,M_{\rm Jup}$ as observations from the WEIRD sample reach sufficient completeness ($> 50\%$) at this mass for the large semimajor axis (> 1000 au). The upper mass limit of $20\,M_{\rm Jup}$ was chosen to exclude the brown dwarf companion population, as RV data suggest a natural dividing line between

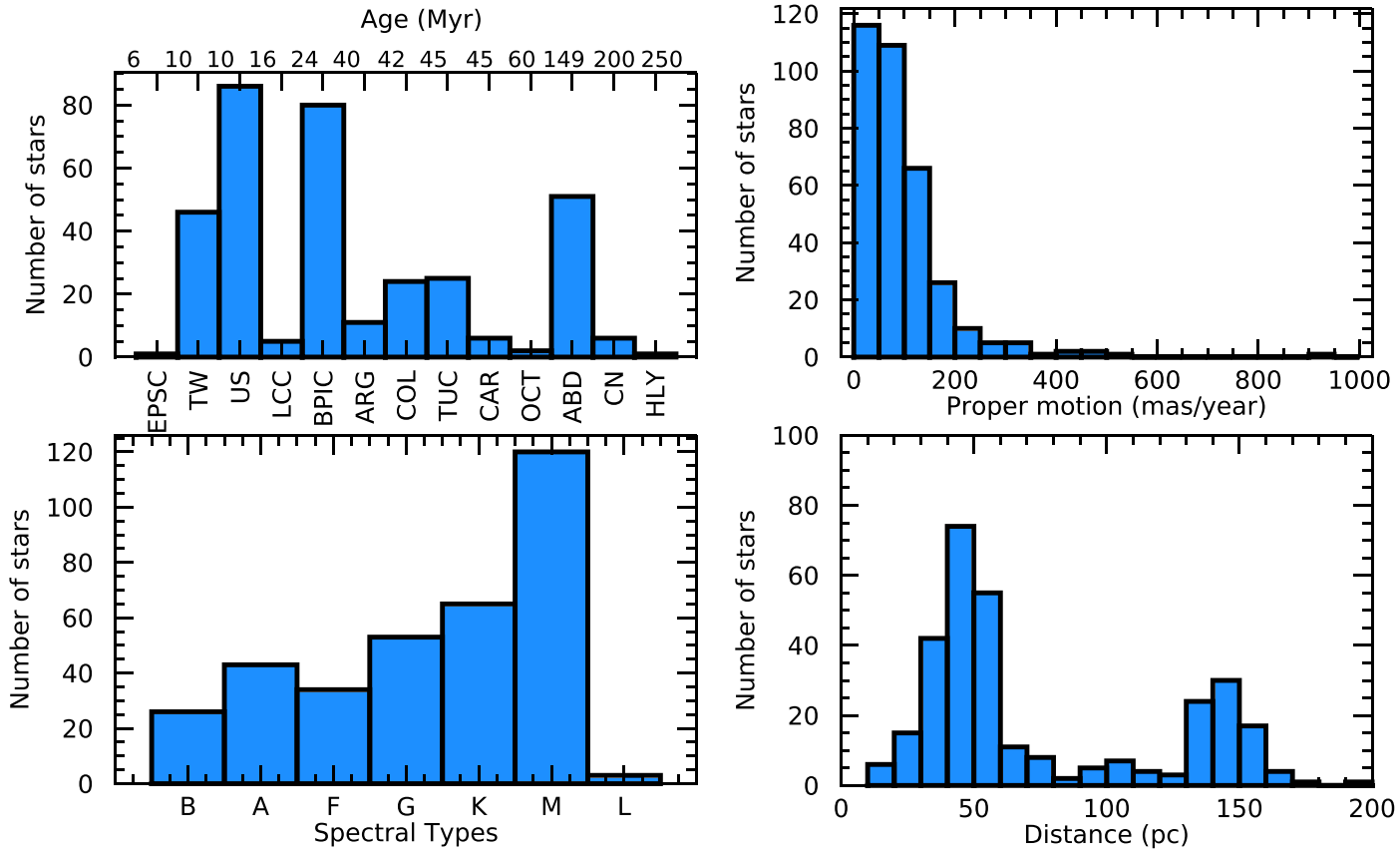

Figure 1. Histograms of the number of stars in each association, distances (pc), proper motions (mas/yr), and spectral types of the targets in the sample.

planets and brown dwarfs somewhere in the 25–45 $M_{\rm Jup}$ range (Sahlmann et al. 2011).

Figure 2 shows the average completeness maps for (a) the 220 objects with WEIRD or PSYM-Wide images (seeing-limited), (b) the 119 targets with only the AO observations from the DIVA archives, (c) the 83 Upper Scorpius targets with only AO observations, and (d) the 73 targets that were observed by AO *and* either WEIRD or PSYM-WIDE. The known companions discussed above are overplotted. Note that the semimajor axis is used when known; otherwise, the projected separation is used as a semimajor axis. The maps show that the AO images are sensitive to companions with masses of about 7 $M_{\rm Jup}$ or higher at a completeness of 70% with a semimajor axis between 50 and 300 au, or a completeness of 50% for semimajor axes larger than 20 au. The seeing-limited observations, on the other hand, are mostly sensitive to semimajor axes above 500 au for masses above 3 $M_{\rm Jup}$ with a completeness of 70%. As panel (d) demonstrates, combining AO imaging with wide-field imaging enables a good semimajor axis coverage as well as a decent companion mass coverage. Panel (e) shows the average completeness maps for the entire survey. Overall, the survey is mostly sensitive to objects more massive than 3 $M_{\rm Jup}$ at semimajor axes between 500 and 1500 au.

3.1. Frequency of Companions

Using the individual completeness maps for all targets in the sample and the statistical formalism presented in Lafrenière et al. (2007), a frequency f of stars that have at least one companion with a mass between 1 and 20 $M_{\rm Jup}$ and a semimajor axis between 20 and 5000 au was evaluated. For this first analysis, we chose to focus on the 20–5000 au range of the semimajor axis, as this is where we reach the most interesting completeness to constrain the occurence rate. Even though we have some sensitivity at smaller separations, extending this analysis to cover smaller separations would lead to larger uncertainties because the completeness is significantly smaller below 20 au. Assuming that N is the total number of stars in the sample and k is the ith star of said sample, then the results of the survey can be summarized by the set $\{d_k\}$, where the value of d_k is 1 if one (or more) companion is detected around star k, and d_k is 0 otherwise. If p_k is the probability that such a star hosts a companion that would be detected given the detection limits of the observations if indeed it was there, then the likelihood of the data for a given value of f is given by the binomial likelihood

$$\mathcal{L}(\{d_k\}|f) = \prod_{k=0}^{N} (1 - fp_k)^{1-d_k}(fp_k)^{d_k}. \quad (1)$$

If $p(f)$ is the prior probability of f, then according to Baye's theorem, the posterior distribution for f, in light of the data, is given by

$$p(f|\{d_k\}) = \frac{\mathcal{L}(\{d_k\}|f)p(f)}{\int_0^1 \mathcal{L}(\{d_k\}|f)p(f)df}. \quad (2)$$

The prior $p(f)$ represents the best knowledge about the posterior distribution of f based only on information that is independent from the current analyses, to apply Bayesian statistics in a way that only depends on the available data and the given likelihood, it is appropriate to use a noninformative

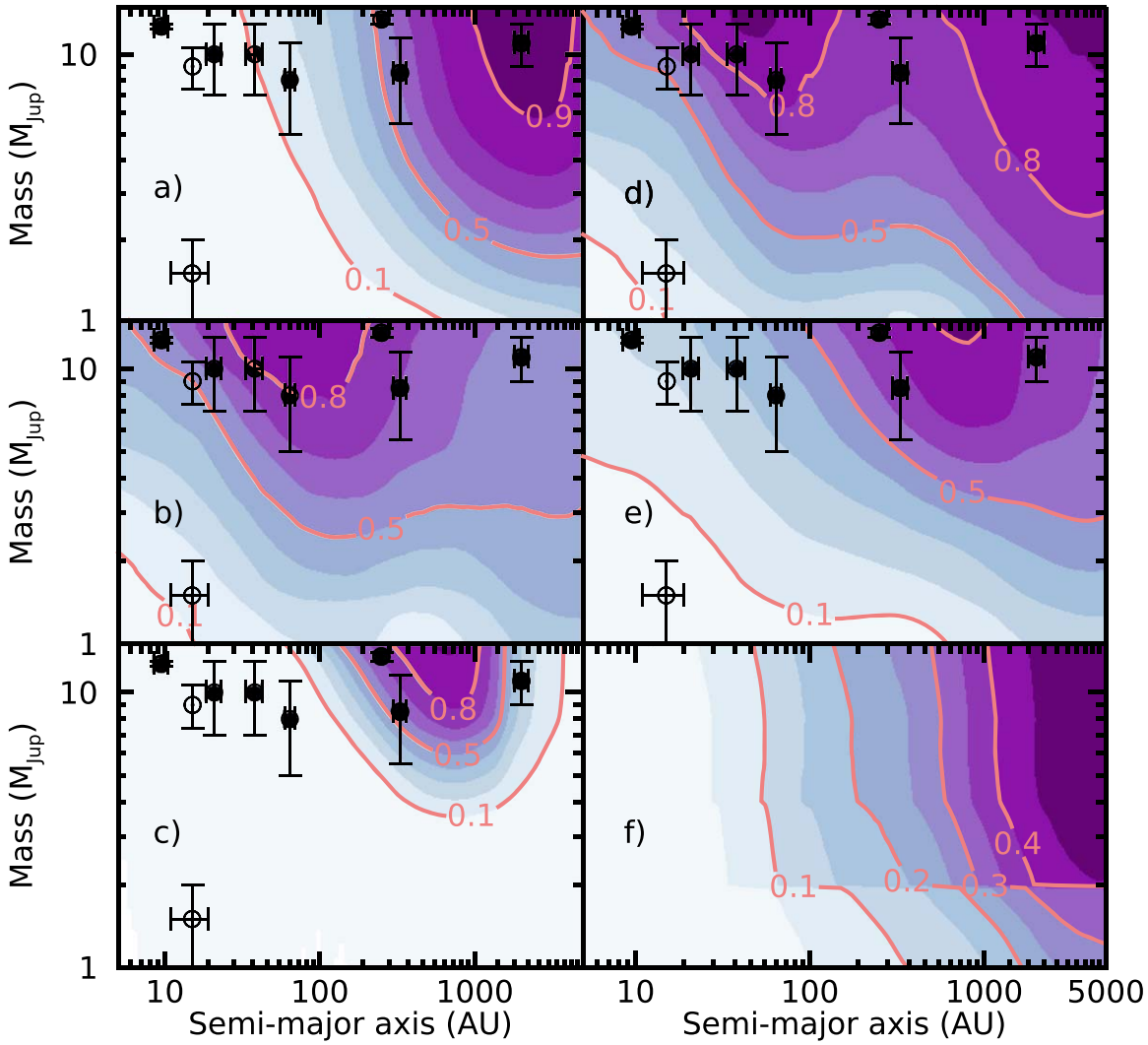

Figure 2. Average detection completeness maps of the masses vs. the semimajor axis. Filled circles show the known companions detected in the observations used in the present study, while open circles show known companions of stars in our sample that were detected by other surveys. The maps show the average probability of detecting a companion with a mass between 1 and 20 $M_{\rm Jup}$ as a function of the separation from the host star. Panel (a) is the average completeness map for the seeing-limited observations (WEIRD and PSYM-WIDE) only, sensitive to larger separations; (b) is for AO observations of nearby young associations, sensitive to shorter orbits; (c) is for AO observations of stars of the more distant Upper Scorpius association, sensitive to intermediate separations; (d) is for the subset of stars in nearby associations that were observed with both seeing-limited observations and AO; (e) is the average completeness map for the overall survey; and (f) is the same as (e) using cold-start models.

prior (Berger et al. 2009). Here, we used a noninformative Jeffrey's prior, which is appropriate for the binomial likelihood, and is given by

$$p(f) = \frac{1}{\pi}\frac{1}{\sqrt{f}}\frac{1}{\sqrt{1-f}}. \quad (3)$$

The maximum of the posterior distribution is obtained for the most likely value for f. An equal-tail credible interval ($\alpha = 0.95$) can be determined from

$$\frac{1-\alpha}{2} = \int_0^{f_{\rm min}} p(f|d_k)df, \quad (4)$$

$$\frac{1+\alpha}{2} = \int_{f_{\rm max}}^1 p(f|d_k)df. \quad (5)$$

We applied the above procedure to constrain f over various semimajor axis intervals and for planet masses from 1 to 20 $M_{\rm Jup}$. To compute p_k we simply averaged the above completeness maps over the appropriate region of semimajor axis and planet mass of our grid; this amounts to assuming the planets are distributed uniformly in logarithm scale in both mass and semimajor axis.

Figure 3 shows the posterior distributions obtained for the full semimajor axis range probed by our study, as well as for two subranges, 20–1000 au and 1000–5000 au. From these posterior distributions, we can infer a frequency of companions with masses between 1 and 20 $M_{\rm Jup}$ for the corresponding ranges of semimajor axes. First, for the 20–1000 au range, which contains the detection of companions around four stars of the sample (AB Pic, HR 8799, HIP 78530 B, and 1RXS J160929.1−210524), we obtained a frequency of $2.17^{+6.85}_{-0.73}$% at a 95% confidence level. For the 1000–5000 au range, which contains only one companion (GU Psc b), we inferred a frequency of $0.3^{+2.6}_{-0.1}$% at a 95% confidence level. This is much lower than at shorter separations, and is easily understood as this range contains much fewer detections despite having better sensitivities on average. For the overall range of semimajor

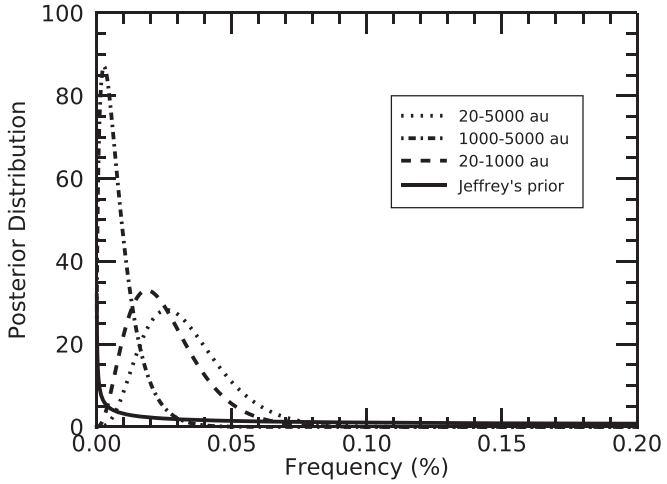

Figure 3. Posterior distributions of the occurrence rate of companions of masses between 1 and 20 $M_{\rm Jup}$. The dotted line shows the frequency in the semimajor axis range of 20–5000 au, the dashed–dotted line is for the range of 1000–5000 au, and the dashed is for the range of 20–1000 au. The solid line shows the Jeffrey's prior used.

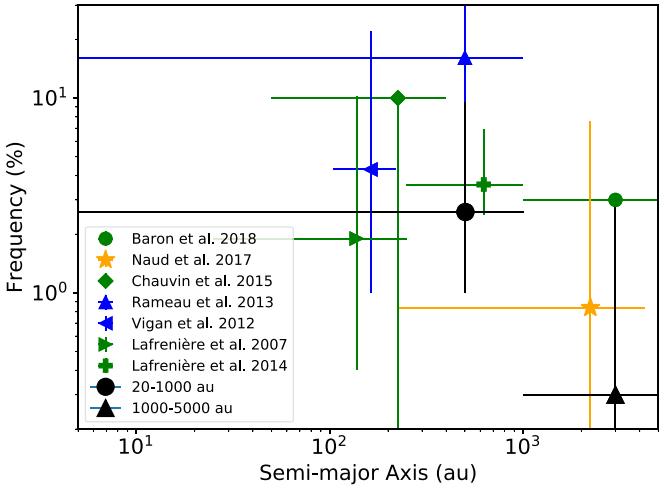

Figure 4. Frequency of companions for various ranges of semimajor axes probed by this study and others. The survey that concentrated on M dwarfs is shown in orange, the studies that surveyed A stars in blue, and the others are shown in green. The frequency from Baron et al. (2018) is represented by a circle, the one from Naud et al. (2017) is drawn as a star, the one from Chauvin et al. (2015) is a diamond, the one from Rameau et al. (2013b) is drawn as a triangle pointing up, the one from Vigan et al. (2012) is shown as a left pointing triangle, the one from Lafrenière et al. (2007) is drawn as a right pointing triangle, and the one for Lafrenière et al. (2014) is represented by a thick plus sign. The frequency from the current analysis is shown as a black square for the range of 20–5000 au, a black triangle for the range of 1000–5000 au, and a dark circle for the range of 20–1000 au. The horizontal bars represent the ranges of semimajor axes, while the vertical error bars show a 95% credible interval for the companion frequency.

axes probed here (20–5000 au) we obtained a frequency of $2.61^{+6.97}_{-1.00}$% at a 95% confidence level.

Figure 4 shows the frequency that we found and those obtained by the individual surveys included in our study over a similar companion mass range and for various ranges of semimajor axes. Here, the horizontal bars represent the ranges of semimajor axes while the vertical error bars correspond to the uncertainty interval on the frequencies (at a 95% confidence level). The surveys included in our sample cover a wide range of spectral types, but some of the other surveys focused on M dwarfs and others on A stars. The surveys in our study that focused on wide orbits (20–1000 au) found overall marginally higher frequencies than those that focused on very wide orbits (1000–5000 au). This is consistent with the frequencies we calculated in both intervals. Table 4 presents, for context, a compilation of several literature results for the occurrence of giant planets based on direct imaging surveys. We can also compare our results directly to others surveys to show that we get similar results. First we compare to the meta-analysis from Bowler (2016). Using the same analysis as previously in the interval of 5–13 $M_{\rm Jup}$ and 30–300 au for all spectral types, we obtain a occurrence of $1.83^{+5.76}_{-0.62}$%, comparable to the overall occurrence rate of Bowler (2016) of $0.6^{+0.5}_{-0.7}$%. We also compare our analysis to studies that targeted M dwarfs, as our survey has a good number of them. In the range of 500–5000 au and 1–13 $M_{\rm Jup}$, Naud et al. (2017) obtained a frequency of $0.84^{+6.73}_{-0.66}$%. For the same range of semimajor axes and masses, we get $0.3^{+2.75}_{-0.06}$%, which is comparable within uncertainties to Naud et al. (2017). We also compare with Galicher et al. (2016) and we obtained an occurrence of $1.79^{+7.5}_{-0.49}$%, comparable to their $1.05^{+2.80}_{-0.70}$% in the range of 1–14 $M_{\rm Jup}$ and 20–300 au.

3.2. Constraining the Distribution of Companions

We used a Markov chain Monte Carlo (MCMC) approach to constrain the distribution of companions as a function of their mass and semimajor axis. We used the same mass–semimajor axis grid in the 5–5000 au interval for the calculation of the completeness maps, and we use index i to refer to a given bin in mass, index j to refer to a given bin in semimajor axis, index s to refer to a given bin in projected separation axis, and index k to refer to a given star out of the total sample of N stars surveyed. The completeness maps as a function of the projected separation, calculated earlier, are noted as $C_{k,is}$. The set $\{d_{k,is}\}$ denotes the detection made by the observations, such that $d_{k,is}$ is 1 if there is a planet detected in bin (i, s) for star k, otherwise $d_{k,is}$ is 0. In our calculations, detected companions were assigned to the projected separation bin s when they were detected in the images used in our study.

As a first case, we assumed that the distribution of planets follows a power law in mass and semimajor axis,

$$d^2n = f\frac{\alpha\beta}{C}M^{\alpha}a^{\beta}dMda, \tag{6}$$

where dn is the expected number of companions with a mass in the range of $[M, M + dM]$ and a semimajor axis in the range of $[a, a + da]$, f is the overall mean number of planets per star (what we also call the frequency of planets), and C is a normalization constant ensuring that the overall expected number of companions per star found by integrating dn over the full mass and the semimajor axis is equal to f.

For a given bin (i, j), the expected number of companions is found by integrating over the bin, which yields,

if $\alpha \neq -1$ and $\beta \neq -1$:

$$n_{i,j} = \frac{f}{D}[M_{i+1}^{\alpha+1} - M_i^{\alpha+1}][a_{i+1}^{\beta+1} - a_i^{\beta+1}], \tag{7}$$

or if $\alpha = -1$ and $\beta = -1$

$$n_{i,j} = \frac{f}{D}\ln\left(\frac{M_{i+1}}{M_i}\right)\ln\left(\frac{a_{i+1}}{a_i}\right), \tag{8}$$

Table 4
Properties of the Sample of Bona Fide Members

Name	RA (J2000.0)	DEC (J2000.0)	SpT	$\mu_\alpha \cos\delta$ (mas/yr)	μ_δ (mas/yr)	Association	Distance (pc)	Masses ($M_\odot$)	Surveys
HIP 490	00 05 52.54	−41 45 11.0	G0V	97.53 ± 0.38	−76.27 ± 0.44	THA	39.385 ± 0.915	1.53	3
HD 203	00 06 50.08	−23 06 27.1	F2IV	96.77 ± 0.13	−47.12 ± 0.06	BPIC	39.960 ± 0.099	1.33	3
HIP 1113	00 13 53.01	−74 41 17.8	G8V	83.53 ± 0.78	−47.89 ± 0.75	THA	44.404 ± 1.616	1.18	3
HD 984	00 14 10.25	−07 11 56.8	F5V	104.53 ± 0.15	−67.91 ± 0.06	COL	45.911 ± 0.118	1.00	3
2MASS J00172353-6645124	00 17 23.53	−66 45 12.4	M2.5	102.90 ± 1.00	−15.00 ± 1.00	ABD	51.241 ± 0.120	1.56	10
V* PW And	00 18 20.89	30 57 22.1	K0Ve	143.19 ± 0.09	−171.11 ± 0.06	ABD	29.450 ± 0.133	0.80	12
HIP 1481	00 18 26.12	−63 28 38.9	F8	90.06 ± 0.05	−59.18 ± 0.05	THA	42.970 ± 0.055	2.00	11
HIP 1910 AB	00 24 08.98	−62 11 04.3	M0Ve	90.34 ± 0.95	−45.14 ± 0.94	THA	44.230 ± 1.066	2.06	9
HIP 1993	00 25 14.66	−61 30 48.2	M0Ve	87.92 ± 0.04	−56.16 ± 0.04	THA	44.163 ± 0.056	0.37	7
GJ 2006 A	00 27 50.23	−32 33 06.4	M3.5V	117.40 ± 2.80	−29.30 ± 8.10	BPIC	32.289 ± 1.834	1.33	2
HIP2484	00 31 32.67	−62 57 29.6	A2V	83.64 ± 0.19	−54.82 ± 0.18	THA	41.407 ± 0.342	0.27	7
bet03 Tuc	00 32 43.90	−63 01 53.4	A0V	86.41 ± 0.21	−50.35 ± 0.21	THA	45.901 ± 0.280	1.16	3
2MASS J00325584-4405058	00 32 55.84	−44 05 05.8	L0γ	128.30 ± 3.40	−93.60 ± 3.00	BPIC	28.335 ± 0.037	1.23	2
HIP 2729	00 34 51.20	−61 54 58.1	K5Ve	88.69 ± 0.04	−52.66 ± 0.03	THA	44.497 ± 0.049	0.25	12
2MASS J00374306-5846229	00 37 43.06	−58 46 22.9	L0γ	57.00 ± 10.00	17.00 ± 5.00	BPIC	75.573 ± 0.185	1.31	3
HIP 3556	00 45 28.15	−51 37 33.9	M3	99.23 ± 0.09	−58.58 ± 0.08	THA	41.160 ± 0.105	2.20	2
HIP 3589	00 45 50.89	54 58 40.2	F8V	96.81 ± 0.65	−74.17 ± 0.53	ABD	52.521 ± 2.455	1.20	2
HIP 4448 A	00 56 55.46	−51 52 31.8	K3Ve	96.24 ± 0.34	10.75 ± 0.29	ARG	37.071 ± 0.274	0.49	12
G132-51 B	01 03 42.11	+40 51 15.8	M2.6V	132.00 ± 5.00	−164.00 ± 5.00	ABD	29.940 ± 1.972	1.16	3
HD 6569 AB	01 06 26.15	−14 17 47.1	K1V	99.92 ± 0.08	−94.62 ± 0.05	ABD	45.433 ± 0.090	0.80	12
2MASS J01112542+1526214	01 11 25.42	15 26 21.5	M5V	180.00 ± 2.00	−120.00 ± 5.00	BPIC	21.800 ± 0.798	1.10	2
2MASS J01123504+1703557	01 12 35.04	17 03 55.7	M3	92.00 ± 1.00	−98.40 ± 1.00	BPIC	46.274 ± 0.184	1.51	3,13
HIP 6276	01 20 32.26	−11 28 03.7	G0V	111.43 ± 0.09	−136.88 ± 0.06	ABD	35.331 ± 0.059	1.60	3
2MASS J01220441-3337036	01 22 04.41	−33 37 03.6	K7	105.30 ± 1.20	−58.30 ± 1.00	BPIC	109.625 ± 0.997	0.93	1
2MUCD 13056	01 23 11.26	−69 21 38.0	M7.5V	77.40 ± 2.40	−25.40 ± 9.00	THA	46.296 ± 7.073	1.06	3
HIP 6485	01 23 21.25	−57 28 50.6	G6V	92.79 ± 0.04	−36.08 ± 0.03	THA	45.314 ± 0.053	1.16	3
G269-153	01 24 27.68	−33 55 08.6	M4.3V	178.00 ± 20.00	−110.00 ± 20.00	ABD	25.125 ± 1.010	0.32	12
HIP 6856	01 28 08.65	−52 38 19.1	K1V	106.14 ± 0.04	−42.98 ± 0.04	THA	39.843 ± 0.044	0.86	12
2MASS J01351393-0712517	01 35 13.92	−07 12 51.7	M4(sb2)	106.50 ± 5.10	−60.70 ± 5.10	BPIC	37.279 ± 0.125	0.80	1,2,7,10,11
G271-110	01 36 55.17	−06 47 37.9	M3.5V	168.00 ± 5.00	−105.00 ± 5.00	BPIC	41.666 ± 0.694	0.80	2
2MASS J01521830-5950168	01 52 18.30	−59 50 16.8	M2-3	109.20 ± 1.80	−25.70 ± 1.80	THA	24.883 ± 0.093	1.95	10
HIP 9141 AB	01 57 48.97	−21 54 05.3	G3V	103.56 ± 0.09	−50.29 ± 0.09	THA	41.411 ± 0.092	1.43	2,10
HIP 9685	02 04 35.13	−54 52 54.0	F2V	75.35 ± 0.09	−25.86 ± 0.07	THA	46.281 ± 0.109	0.98	12
2MASS J02045317-5346162	02 04 53.17	−53 46 16.2	K5	95.10 ± 2.90	−33.60 ± 3.10	BPIC	101.081 ± 0.378	0.20	12
2MASS J02070176-4406380	02 07 01.98	−44 06 44.4	M3.5(sb1)	94.90 ± 1.30	−30.60 ± 1.30	TWA	30.346 ± 0.052	0.84	12
HIP 9892	02 07 18.06	−53 11 56.5	G7V	86.06 ± 0.58	−22.60 ± 0.65	THA	50.942 ± 1.660	0.89	12
HIP 9902	02 07 26.12	−59 40 45.9	F8V	92.58 ± 0.04	−18.26 ± 0.04	THA	45.610 ± 0.056	0.15	12
HIP 10272	02 12 15.41	23 57 29.5	K1V	125.44 ± 1.45	−161.47 ± 0.98	ABD	36.630 ± 1.596	1.65	1,5,7
HD 14228 A	02 16 30.58	−51 30 43.7	B8IV	90.23 ± 0.49	−22.85 ± 0.49	THA	46.095 ± 0.724	1.04	12
* gam Tri	02 17 18.86	33 50 49.9	A1	45.35 ± 0.70	−51.61 ± 0.63	OCT	28.679 ± 0.060	0.65	6
HIP 10679	02 17 24.74	28 44 30.4	G2V	80.15 ± 4.38	−78.40 ± 4.91	BPIC	27.337 ± 4.356	1.23	6
2MASS J02215494-5412054	02 21 54.94	−54 12 05.4	M8beta	136.00 ± 10.00	−10.00 ± 17.00	TWA	28.679 ± 0.060	0.68	12
2MASS J02224418-6022476	02 22 44.18	−60 22 47.6	M4	137.40 ± 1.70	−13.80 ± 1.70	TWA	49.615 ± 0.083	2.13	11
HIP 11152	02 23 26.64	22 44 06.7	M3V	92.43 ± 3.05	−113.69 ± 2.36	BPIC	28.686 ± 2.337	0.16	12
HD 15115	02 26 16.24	06 17 33.1	F4IV	88.03 ± 0.07	−50.51 ± 0.07	BPIC	49.002 ± 0.100	0.01	12
HIP 11437	02 27 29.25	30 58 24.6	K8V	79.78 ± 2.56	−70.02 ± 1.73	BPIC	39.952 ± 3.591	0.42	12
1RXS J022735.8+471021	02 27 37.26	47 10 04.5	M4.6V	119.00 ± 5.00	−183.00 ± 5.00	ABD	36.509 ± 3.079	0.55	12

Table 4
(Continued)

Name	RA (J2000.0)	DEC (J2000.0)	SpT	$\mu_\alpha \cos\delta$ (mas/yr)	μ_δ (mas/yr)	Association	Distance (pc)	Masses ($M_\odot$)	Surveys
2MASS J02340093-6442068	02 34 00.92	−64 42 06.8	L0γ	88.00 ± 12.00	−15.00 ± 12.00	TWA	48.213 ± 0.134	0.74	12
HIP 12394	02 39 35.35	−68 16 01.0	B9V	87.33 ± 0.43	0.38 ± 0.46	THA	47.357 ± 0.538	0.27	12
V* s Eri	02 39 47.98	−42 53 30.0	A1V	125.80 ± 0.57	−11.61 ± 0.62	COL	40.472 ± 0.643	0.58	12
BD+05 378	02 41 25.88	05 59 18.4	K6Ve	79.12 ± 0.09	−56.61 ± 0.10	BPIC	44.436 ± 0.154	0.01	12
V* AF Hor	02 41 47.31	−52 59 30.7	M2V	92.20 ± 1.10	−4.20 ± 1.50	THA	40.000 ± 0.800	0.74	12
HIP 12635	02 42 20.95	38 37 21.5	K3.5V	75.73 ± 2.49	−111.45 ± 2.73	ABD	50.428 ± 6.662	1.00	4,6
HIP 12925	02 46 14.61	+05 35 33.3	F8V	75.27 ± 1.45	−44.78 ± 0.83	THA	54.318 ± 3.068	0.44	12
HIP 13027	02 47 27.24	19 22 18.5	G0V	117.91 ± 0.89	−161.81 ± 0.71	ABD	33.557 ± 0.923	0.31	12
2MASS J02485260-3404246	02 48 52.60	−34 04 24.6	M4(sb1)	90.20 ± 1.40	−23.70 ± 1.40	BPIC	43.376 ± 0.211	0.86	3
HIP 13209	02 49 59.03	27 15 37.8	B8V	66.81 ± 0.24	−116.52 ± 0.15	ABD	50.787 ± 0.490	2.00	10,11
2MASS J02564708-6343027	02 56 47.08	−63 43 02.7	M4	67.40 ± 2.20	8.30 ± 5.60	BPIC	45.269 ± 0.104	0.83	2
HIP 14551	03 07 50.85	−27 49 52.1	A5V	66.26 ± 0.50	−19.09 ± 0.49	THA	54.644 ± 1.493	0.28	12
V* IS Eri	03 09 42.28	−09 34 46.5	G0V	89.85 ± 0.08	−112.54 ± 0.07	ABD	38.705 ± 0.065	0.06	12
HIP 14807	03 11 12.33	22 25 22.7	K6V	54.86 ± 3.99	−134.25 ± 3.87	ABD	40.160 ± 2.064	1.18	3
HIP 14913	03 12 25.75	−44 25 10.8	A8V+F3V	81.63 ± 0.55	−4.57 ± 0.98	THA	42.498 ± 1.119	0.29	12
HIP 15247	03 16 40.67	−03 31 48.9	F6V	82.10 ± 0.08	−49.08 ± 0.08	THA	48.766 ± 0.123	0.09	12
HIP 15353	03 17 59.07	−66 55 36.7	A3V	56.94 ± 0.30	12.68 ± 0.40	ABD	54.945 ± 0.905	0.93	4,5,10
CD-35 1167	03 19 08.66	−35 07 00.3	K7V	89.20 ± 2.80	−20.30 ± 2.80	THA	45.289 ± 0.738	0.13	12
CD-46 1064	03 30 49.09	−45 55 57.3	K3V	88.54 ± 0.03	−4.95 ± 0.04	THA	42.687 ± 0.158	0.02	12
CD-44 1173	03 31 53.64	−25 36 50.9	A3V	54.13 ± 0.05	−15.17 ± 0.06	COL	9.831 ± 0.009	0.43	12
CD-441173	03 31 55.64	−43 59 13.5	K6V	90.90 ± 1.90	−5.00 ± 1.90	THA	45.248 ± 0.614	2.00	11
V577 Per	03 33 13.49	46 15 26.5	G5V	68.46 ± 0.96	−176.81 ± 0.76	ABD	34.387 ± 1.206	1.50	10,11
2MASS J03350208+2342356	03 35 02.08	23 42 35.6	M8.5	54.00 ± 10.00	−56.00 ± 10.00	BPIC	51.209 ± 0.404	0.80	12
HIP 16853	03 36 53.40	−49 57 28.9	G2V	89.74 ± 0.75	0.29 ± 0.84	THA	43.346 ± 1.371	0.44	12
HIP 17248	03 41 37.24	55 13 06.8	M0.5V	96.17 ± 2.49	−117.69 ± 2.26	COL	35.211 ± 2.702	1.15	3
HIP 17695	03 47 23.43	−01 58 19.9	M2.5V	185.53 ± 3.77	−273.48 ± 3.95	ABD	16.129 ± 0.749	0.01	12
HIP 17764	03 48 11.47	−74 41 38.8	F3V	63.46 ± 0.39	24.86 ± 0.49	THA	54.054 ± 1.168	0.11	12
HIP 17782	03 48 23.00	52 02 16.3	G8V	61.87 ± 1.98	−70.99 ± 1.67	THA	51.679 ± 4.326	1.25	3
HIP 17797	03 48 35.88	−37 37 12.5	A1V	74.44 ± 0.71	−9.09 ± 0.87	THA	50.735 ± 2.213	0.89	1,2
HD 25284	04 00 03.83	−29 02 16.4	K4.6	72.52 ± 0.18	−12.47 ± 0.17	THA	9.831 ± 0.009	0.80	12
HIP 18714	04 00 31.99	−41 44 54.4	G3V	69.46 ± 0.81	−7.00 ± 0.85	THA	48.496 ± 1.669	0.91	12
HD 25457	04 02 36.74	00-16 08.1	F5V	149.18 ± 0.19	−251.67 ± 0.08	ABD	18.771 ± 0.040	1.00	1,2
HD 25953	04 06 41.53	01 41 02.0	F5V	36.46 ± 0.08	−94.67 ± 0.05	ABD	56.963 ± 0.146	0.36	12
2MASS J04082685-7844471	04 08 26.85	−78 44 47.1	M0	54.70 ± 1.40	42.10 ± 1.40	BPIC	32.226 ± 0.093	2.20	10
2MASS J04091413-4008019	04 09 14.13	−40 08 01.9	M3.5	45.90 ± 1.70	7.20 ± 1.70	BPIC	24.245 ± 0.029	1.00	2
1RXS J041417.0-090650	04 14 17.30	−09 06 54.4	M4.3V	96.00 ± 10.00	−138.00 ± 10.00	ABD	23.809 ± 1.417	0.00	12
HIP 19775	04 14 22.56	−38 19 01.5	G3V	40.04 ± 0.03	2.18 ± 0.04	COL	18.128 ± 0.020	0.76	12
2MASS J04213904-7233562	04 21 39.04	−72 33 56.2	M2.5	62.20 ± 1.30	26.60 ± 1.30	BPIC	44.348 ± 0.097	1.00	3
2MASS J04363294-7851021	04 36 32.94	−78 51 02.1	M4	33.00 ± 3.00	47.00 ± 2.70	BPIC	33.952 ± 0.466	1.53	9
51 Eri	04 37 36.13	−02 28 24.7	F0V	44.35 ± 0.22	−63.83 ± 0.17	BPIC	29.782 ± 0.119	1.12	3
GJ 3305 AB	04 37 37.46	−02 29 28.4	M0Ve	59.58 ± 0.71	−52.41 ± 0.61	BPIC	40.490 ± 0.128	0.68	2,5
HIP 21632	04 38 43.94	−27 02 01.8	G3V	56.14 ± 0.04	−10.87 ± 0.04	THA	54.510 ± 0.083	1.10	3
2MASS J04402325-0530082	04 40 23.25	−05 30 08.2	M7	320.40 ± 10.60	126.80 ± 7.30	BPIC	37.835 ± 0.399	0.86	5
HIP 21965	04 43 17.20	−23 37 42.0	F2V	48.71 ± 0.68	1.25 ± 0.70	THA	67.585 ± 1.539	0.86	3
2MASS J04433761+0002051	04 43 37.60	00 02 05.1	M9γ	28.00 ± 14.00	−99.00 ± 14.00	BPIC	28.218 ± 0.030	0.21	2
2MASS J04440099-6624036	04 44 00.96	−66 24 07.5	M0.5	51.60 ± 2.60	33.30 ± 2.60	BPIC	46.048 ± 0.049	0.41	6,7
HD 30422	04 46 25.74	−28 05 14.8	A3	−5.10 ± 0.06	17.52 ± 0.07	OCT	23.658 ± 0.044	0.94	2

Table 4
(Continued)

Name	RA (J2000.0)	DEC (J2000.0)	SpT	$\mu_\alpha \cos\delta$ (mas/yr)	μ_δ (mas/yr)	Association	Distance (pc)	Masses ($M_\odot$)	Surveys
HIP 22226	04 46 49.52	−26 18 08.8	F3V	33.61 ± 0.06	−5.13 ± 0.07	COL	44.677 ± 0.098	0.65	2
2MASS J04480066-5041255	04 48 00.66	−50 41 25.5	K7	53.10 ± 2.10	15.70 ± 2.30	BPIC	45.386 ± 0.085	0.20	7
HIP 22295	04 48 05.17	−80 46 45.3	F7V	46.66 ± 0.49	41.30 ± 0.56	THA	61.012 ± 1.898	0.89	7
2MASS J04533054-5551318	04 53 31.19	−55 51 37.2	M3Ve+M3Ve	134.53 ± 2.39	72.68 ± 2.03	BPIC	11.095 ± 0.003	0.66	2
2MASS J04571728-06215648	04 57 17.28	−06 21 56.4	M0.5	22.90 ± 1.90	−99.10 ± 2.50	BPIC	48.051 ± 1.647	0.83	1,2
HIP 23179	04 59 15.43	37 53 25.1	A1V	46.35 ± 0.63	−97.80 ± 0.41	COL	52.273 ± 2.158	1.23	10
HIP 23362	04 59 15.43	37 53 25.1	A1V	46.35 ± 0.63	−97.80 ± 0.41	COL	52.273 ± 2.158	1.12	1,2
V* V1005 Ori	04 59 34.83	01 47 00.6	M0Ve	39.23 ± 0.06	−95.05 ± 0.29	BPIC	24.401 ± 0.020	1.45	9
CD-57 1054	05 00 47.12	−57 15 25.4	M0.5e	35.19 ± 0.04	74.13 ± 0.05	BPIC	26.900 ± 0.020	0.94	1,2
HIP 23316	05 00 51.86	−41 01 06.7	G5V	31.52 ± 0.03	10.22 ± 0.05	COL	36.805 ± 0.047	0.44	12
HIP 23418	05 01 58.79	09 58 59.3	M3V	12.09 ± 9.92	−74.41 ± 5.71	BPIC	24.888 ± 1.282	1.10	2,7
GJ3331	05 06 49.91	−21 35 09.1	M1V	34.20 ± 1.20	−33.80 ± 2.10	BPIC	19.193 ± 0.515	0.58	6
V* AS Col	05 20 38.04	−39 45 17.7	F6V	38.67 ± 0.05	12.90 ± 0.07	COL	47.662 ± 0.072	1.43	2,10
2MASS J05241317-2104427	05 24 13.17	−21 04 42.7	M4	33.30 ± 2.50	−17.10 ± 2.20	BPIC	28.335 ± 0.037	1.80	1,2,7,10,11,14
HD 35650 AB	05 24 30.16	−38 58 10.7	K6e	43.02 ± 0.04	−57.33 ± 0.05	ABD	17.479 ± 0.008	1.11	2,7
CD-43 1846	05 26 22.96	−43 22 36.2	G0	20.36 ± 0.04	10.90 ± 0.05	COL	42.004 ± 0.206	1.18	1
V* AF Lep	05 27 04.76	−11 54 03.4	F7	17.05 ± 0.04	−49.31 ± 0.04	BPIC	26.877 ± 0.018	4.50	10
AB Dor Bab	05 28 44.46	−65 26 46.3	M5Ve	66.36 ± 0.15	125.89 ± 0.18	ABD	14.919 ± 0.020	1.40	9,10
AB Dor Aab	05 28 44.84	−65 26 54.9	K2V	29.15 ± 0.25	164.42 ± 0.29	ABD	59.953 ± 0.323	2.20	2
2MASS J05332558-5117131	05 33 25.58	−51 17 13.1	K7	43.80 ± 2.10	25.10 ± 2.10	BPIC	43.923 ± 0.044	1.43	3,10,11
2MASS J05335981-0221325	05 33 59.81	−02 21 32.5	M3	12.30 ± 1.20	−61.30 ± 2.40	BPIC	69.642 ± 0.194	1.53	9,10
HD 37286	05 36 10.29	−28 42 28.8	A2III-IV	25.32 ± 0.05	−3.08 ± 0.07	COL	58.896 ± 0.152	1.30	2,9
HIP 26369	05 36 55.10	−47 57 48.1	K6V	24.05 ± 2.62	13.08 ± 1.82	ABD	25.634 ± 4.823	0.53	1,5,7
UY Pic	05 36 56.85	−47 57 52.8	K0V	22.97 ± 0.04	−1.13 ± 0.05	ABD	69.642 ± 0.194	1.03	2
HD 37484	05 37 39.62	−28 37 34.6	F3	24.08 ± 0.03	−3.10 ± 0.04	COL	59.112 ± 0.083	1.36	2,10
2MASS J05395494-1307598	05 39 54.94	−13 07 59.8	M3	20.30 ± 4.80	−11.70 ± 5.40	BPIC	69.642 ± 0.194	1.50	2
HIP 26966	05 43 21.66	−18 33 26.9	A0V	19.35 ± 0.10	−13.75 ± 0.12	COL	49.380 ± 0.248	3.50	3,10
HIP 26990	05 43 35.80	−39 55 24.6	G0V	25.82 ± 0.32	15.08 ± 0.52	COL	55.370 ± 1.379	1.86	10
Beta Pic	05 47 17.08	−51 03 59.4	A6V	2.49 ± 0.68	82.57 ± 0.68	BPIC	19.753 ± 0.130	2.50	10,11
HD 42270	05 53 29.31	−81 56 53.1	K0V	25.26 ± 0.06	63.38 ± 0.06	CAR	57.709 ± 0.085	1.14	5
HIP 28036	05 55 43.16	−38 06 16.2	F7V	20.69 ± 0.04	9.96 ± 0.04	COL	52.828 ± 0.069	1.06	3
HD 41071	06 00 41.29	−44 53 50.1	G8	18.15 ± 0.05	23.26 ± 0.05	COL	54.392 ± 0.085	2.50	10
AP Col	06 04 52.15	−34 33 36.0	M5V	27.33 ± 0.35	340.92 ± 0.35	ARG	8.388 ± 0.068	2.13	10
2MASS J06085283-2753583	06 08 52.84	−27 53 58.4	M8.5V	8.90 ± 3.50	10.70 ± 3.50	BPIC	31.250 ± 3.515	1.46	3,10,11
CD-35 2722	06 09 19.21	−35 49 31.2	M1V	−6.30 ± 2.80	−56.60 ± 2.80	ABD	21.276 ± 1.358	2.70	3,10
2MASS J06112997-7213388	06 11 29.97	−72 13 38.8	M4+M5	23.20 ± 1.60	60.20 ± 1.70	BPIC	79.732 ± 0.146	2.13	11
2MASS J06131330-2742054	06 13 13.31	−27 42 05.5	M4V	−14.90 ± 1.00	−2.10 ± 1.00	BPIC	29.377 ± 0.863	1.30	1,2,5
V* AO Men	06 18 28.20	−72 02 41.4	K4Ve	−7.90 ± 0.04	74.29 ± 0.05	BPIC	39.261 ± 0.038	0.84	1
HIP 30030	06 19 08.05	−03 26 20.3	G0V	10.70 ± 0.08	−42.29 ± 0.08	COL	52.012 ± 0.148	1.23	3
AB Pic	06 19 12.91	−58 03 15.5	K1V(e)	14.33 ± 0.06	45.07 ± 0.06	CAR	50.120 ± 0.072	1.36	9
HD 45270 AB	06 22 30.94	−60 13 07.1	G1V	−11.60 ± 0.05	64.43 ± 0.05	ABD	23.889 ± 0.014	0.07	12
CD-40 2458	06 26 06.91	−41 02 53.7	K0V	4.24 ± 0.03	12.56 ± 0.03	COL	53.781 ± 0.098	0.72	5
AK Pic AB	06 38 00.38	−61 32 00.2	G1.5V	−51.98 ± 0.80	69.24 ± 0.67	ABD	20.917 ± 0.122	0.69	5
CD-61 1439 A	06 39 50.02	−61 28 41.5	K7V	−27.30 ± 0.05	74.99 ± 0.05	ABD	22.241 ± 0.014	1.40	4,6,9,10
HIP 32104	06 42 24.31	17 38 43.0	A2V	7.87 ± 0.66	−84.32 ± 0.48	COL	43.630 ± 1.275	1.40	9
HIP 32235	06 43 46.22	−71 58 35.4	G6V	7.36 ± 0.05	60.60 ± 0.08	CAR	55.586 ± 0.101	1.60	4,5,10
HIP 32435	06 46 13.54	−83 59 29.5	F5V	19.66 ± 0.43	61.60 ± 0.47	THA	56.022 ± 1.129	1.18	2

Table 4
(Continued)

Name	RA (J2000.0)	DEC (J2000.0)	SpT	$\mu_\alpha \cos\delta$ (mas/yr)	μ_δ (mas/yr)	Association	Distance (pc)	Masses ($M_\odot$)	Surveys
HIP 33737	07 00 30.46	−79 41 45.9	K2V	1.56 ± 0.94	59.94 ± 1.00	CAR	58.823 ± 3.079	1.53	9
HD 57852	07 20 21.40	−52 18 41.4	F2	−37.70 ± 0.58	148.38 ± 0.55	CN	33.151 ± 0.236	0.15	12
BD+20 1790	07 23 43.59	+20 24 58.7	K5V	−65.80 ± 1.60	−228.10 ± 1.70	ABD	25.773 ± 1.328	0.73	1,6,7,12
GJ2060C	07 25 51.18	−30 15 52.8	M5.0V	−130.00 ± 10.00	−180.00 ± 10.00	ABD	14.903 ± 0.710	0.79	1,5,7
HD 59704	07 29 31.41	−38 07 21.5	F7	−27.40 ± 0.05	68.04 ± 0.05	CN	33.151 ± 0.236	2.20	10
HD 61005	07 35 47.44	−32 12 14.0	G8V	−55.11 ± 0.05	74.14 ± 0.05	ARG	36.485 ± 0.042	0.80	5,7
HD 62850	07 42 36.04	−59 17 50.7	G2.5	−53.90 ± 0.05	158.49 ± 0.05	CN	33.151 ± 0.236	1.36	9
HD 63608	07 46 16.94	−59 48 34.1	K0	−52.46 ± 0.05	153.02 ± 0.05	CN	53.370 ± 0.096	0.69	2
HR 3070	07 49 12.88	−60 17 01.2	F1	−81.65 ± 0.14	166.98 ± 0.13	CN	53.370 ± 0.096	1.37	5,10
2MASS J08173943-8243298	08 17 39.43	−82 43 29.8	M3.5+	−80.30 ± 1.10	102.50 ± 0.80	BPIC	32.912 ± 0.028	0.34	1,2
HIP 47135	09 36 17.83	−78 20 41.7	G1V	−74.85 ± 0.59	50.62 ± 0.59	ARG	67.980 ± 2.772	2.06	11
TWA 21	10 13 14.75	−52 30 53.9	K3	−62.89 ± 0.05	9.50 ± 0.04	CAR	53.350 ± 0.091	1.50	8,10
HIP 50191	10 14 44.16	−42 07 18.9	A2V	−150.09 ± 0.10	49.44 ± 0.11	ARG	31.075 ± 0.144	1.83	2,10
TWA 22 A	10 17 26.87	−53 54 26.4	M5	−173.09 ± 0.55	−4.93 ± 0.54	BPIC	19.606 ± 0.114	1.33	9
BD+01 2447	10 28 55.53	00 50 27.6	M2V	−603.00 ± 0.08	−732.07 ± 0.05	ABD	7.032 ± 0.002	1.10	2
HD 95429	11 00 08.25	−51 49 04.0	A3III-IV	−64.92 ± 0.07	1.69 ± 0.06	LCC	33.805 ± 0.029	0.94	1,5
TWA 1	11 01 51.91	−34 42 17.0	K6V	−66.19 ± 1.85	−13.90 ± 1.47	TWA	53.705 ± 6.172	1.25	10
TWA 43	11 08 43.99	−28 04 50.4	A2Vn	−70.00 ± 0.26	−22.57 ± 0.23	TWA	33.805 ± 0.029	0.94	1,2,10
TWA 2	11 09 13.81	−30 01 39.8	M2V	−95.50 ± 2.90	−23.50 ± 2.80	TWA	46.554 ± 2.817	1.20	1,2,10
TWA 12	11 21 05.49	−38 45 16.3	M2IVe	−62.89 ± 0.05	−14.67 ± 0.04	TWA	65.492 ± 0.154	1.20	1
TWA 13	11 21 17.24	−34 46 45.5	M1V	−66.40 ± 2.40	−12.50 ± 1.80	TWA	55.617 ± 2.227	0.67	2
TWA 4	11 22 05.29	−24 46 39.8	K4V	−85.40 ± 1.73	−33.10 ± 2.12	TWA	44.903 ± 4.657	0.17	14
TWA 5	11 31 55.26	−34 36 27.2	M2V	−81.60 ± 2.50	−29.40 ± 2.40	TWA	50.075 ± 1.755	1.20	14
TWA 30	11 32 18.31	−30 19 51.8	M5V	−89.60 ± 1.30	−25.80 ± 1.30	TWA	23.809 ± 1.133	0.51	14
TWA 8 B	11 32 41.15	−26 52 09.0	M6γ	−90.75 ± 0.17	−23.97 ± 0.11	TWA	46.459 ± 0.248	0.76	14
TWA 8 A	11 32 41.23	−26 51 55.9	M3IVe	−90.64 ± 0.14	−27.41 ± 0.09	TWA	33.766 ± 0.072	0.72	14
TWA 27	11 39 51.14	−31 59 21.5	M9V	−88.00 ± 9.00	−34.00 ± 10.00	TWA	41.981 ± 4.547	0.60	14
TWA 19 A	11 47 24.52	−49 53 03.0	G5	−34.62 ± 0.04	−9.79 ± 0.03	LCC	26.538 ± 0.513	0.00	14
TWA 9 B	11 48 23.71	−37 28 48.5	M1	−56.98 ± 0.08	−15.93 ± 0.06	TWA	58.837 ± 0.131	2.20	14
TWA 9 A	11 48 24.21	−37 28 49.1	K7IVe	−52.96 ± 0.06	−18.46 ± 0.04	TWA	76.376 ± 0.344	1.16	14
HIP 57632	11 49 03.66	14 34 19.7	A3V	−497.68 ± 0.87	−114.67 ± 0.44	ARG	10.999 ± 0.062	1.86	14
HD 103742	11 56 42.31	−32 16 05.3	G3	−171.61 ± 0.07	−8.25 ± 0.04	CN	58.837 ± 0.131	2.20	14
V* T Cha	11 57 13.51	−79 21 31.5	K0	−41.99 ± 0.11	−9.24 ± 0.08	EPSC	53.084 ± 0.532	0.65	14
TWA 23 A	12 07 27.35	−32 47 00.3	M3Ve	−72.77 ± 0.12	−25.88 ± 0.06	TWA	55.669 ± 0.300	1.35	14
TWA 27	12 07 33.47	−39 32 54.0	M8V	−71.60 ± 6.70	−22.10 ± 8.50	TWA	52.631 ± 1.108	0.50	14
TWA 25	12 15 30.72	−39 48 42.5	K9IV-Ve	−76.85 ± 0.09	−28.26 ± 0.04	TWA	53.109 ± 0.186	0.37	14
CD-62 657	12 28 25.39	−63 20 58.8	G7V	−37.39 ± 0.04	−11.41 ± 0.04	LCC	113.404 ± 0.437	0.59	14
TWA 11 C	12 35 48.94	−39 50 24.6	M4V	−45.10 ± 2.40	−20.10 ± 2.30	TWA	69.013 ± 2.429	1.30	14
TWA 11 A	12 36 01.03	−39 52 10.2	A0	−55.65 ± 0.18	−23.74 ± 0.23	TWA	113.404 ± 0.437	0.40	14
CPD-63 2367	12 36 38.97	−63 44 43.5	K1IV	−42.38 ± 0.13	−12.39 ± 0.10	LCC	76.569 ± 0.469	0.36	14
2MASS J12383713-2703348	12 38 37.12	−27 03 34.8	M2.5+	−185.10 ± 5.10	−185.20 ± 5.10	BPIC	35.513 ± 0.052	0.94	14
GJ 490	12 57 40.30	35 13 30.6	M0.5V	−269.00 ± 5.00	−149.00 ± 5.00	THA	18.115 ± 1.017	0.84	14
CD-69 1055	12 58 25.58	−70 28 49.1	K2IV	−41.00 ± 0.04	−16.45 ± 0.04	LCC	35.513 ± 0.052	1.23	14
V* PX Vir	13 03 49.65	−05 09 42.5	G5V	−191.13 ± 0.86	−218.73 ± 0.68	ABD	21.691 ± 0.381	4.50	14
GJ 1167	13 09 34.95	28 59 06.6	M4.8	−332.00 ± 5.00	−210.00 ± 5.00	CAR	11.494 ± 2.391	0.69	14
2MASS J13444279-6347495	13 44 42.79	−63 47 49.4	K4Ve	−35.55 ± 0.04	−23.39 ± 0.05	LCC	47.614 ± 0.163	2.00	14
HD 123058	14 07 29.27	−61 33 44.2	F4	−68.93 ± 0.03	−29.87 ± 0.05	ARG	71.694 ± 0.174	1.13	14

Table 4
(Continued)

Name	RA (J2000.0)	DEC (J2000.0)	SpT	$\mu_\alpha \cos\delta$ (mas/yr)	μ_δ (mas/yr)	Association	Distance (pc)	Masses ($M_\odot$)	Surveys
HIP 74405	15 12 23.43	−75 15 15.6	G9V	−73.87 ± 0.87	−73.08 ± 0.92	ARG	50.301 ± 2.682	0.43	14
HIP 76310	15 35 16.10	−25 44 02.9	A0V	−18.10 ± 0.11	−23.54 ± 0.09	US	137.415 ± 1.074	0.27	14
1RXS J153557.0-232417	15 35 57.80	−23 24 04.5	K3:	−13.64 ± 0.07	−23.49 ± 0.05	US	163.797 ± 0.979	0.69	14
V343 Nor A	15 38 57.52	−57 42 27.2	K0V	−55.19 ± 0.08	−95.88 ± 0.09	BPIC	40.105 ± 0.102	0.51	14
HIP 76633	15 39 00.05	−19 43 57.2	B9V	−15.29 ± 0.10	−18.21 ± 0.07	US	161.470 ± 1.527	0.75	14
HIP 76768	15 40 28.39	−18 41 46.2	K3V	−70.13 ± 3.32	−159.81 ± 2.39	ABD	40.192 ± 4.345	0.22	14
CD-24 12231	15 41 31.20	−25 20 36.3	G9IVe	−17.35 ± 0.08	−25.95 ± 0.05	US	107.956 ± 0.349	1.13	14
SAO 183706	15 41 31.21	−25 20 36.3	G8e	−17.35 ± 0.08	−25.95 ± 0.05	US	130.407 ± 0.636	0.84	14
1RXS J154413.0-252307	15 44 13.34	−25 22 59.1	M1	−15.47 ± 0.11	−24.24 ± 0.08	US	146.284 ± 1.243	1.23	14
HIP 77457	15 48 52.12	−29 29 00.3	A7IV	−7.42 ± 0.10	−18.97 ± 0.06	US	125.879 ± 1.025	0.74	14
HIP 77635	15 50 58.74	−25 45 04.6	B1.5V	−14.57 ± 0.39	−24.64 ± 0.30	US	145.024 ± 5.127	1.20	14
HIP 77840	15 53 36.72	−25 19 37.7	B2.5V	−15.30 ± 0.52	−24.75 ± 0.45	US	161.352 ± 8.479	0.68	14
HIP 77858	15 53 53.91	−24 31 59.3	B5V	−13.74 ± 0.29	−25.04 ± 0.20	US	151.276 ± 3.620	5.50	14
HIP 77859	15 53 55.86	−23 58 41.1	B2V	−13.46 ± 0.29	−23.97 ± 0.20	US	141.294 ± 2.894	0.57	14
1RXS J155405.2-292032	15 54 03.58	−29 20 15.4	M0	−13.10 ± 0.15	−21.69 ± 0.09	US	146.083 ± 1.961	1.13	14
HIP 77900	15 54 30.10	−27 20 19.0	B7V	−13.35 ± 0.18	−25.27 ± 0.11	US	151.430 ± 2.742	0.59	14
HD 142361	15 54 59.86	−23 47 18.1	G3V	−32.67 ± 0.26	−41.67 ± 0.16	US	80.525 ± 1.062	1.13	14
ScoPMS 13	15 56 29.41	−23 48 19.8	M1.5V	−24.32 ± 1.42	−29.88 ± 1.40	US	83.607 ± 5.742	1.15	14
HIP 78104	15 56 53.07	−29 12 50.6	B2IV/V	−18.07 ± 0.69	−24.38 ± 0.58	US	133.481 ± 7.233	1.00	14
[PZ99] J155716.6-2529	15 57 16.74	−25 29 19.3	M0	−14.56 ± 1.35	−17.69 ± 1.30	US	171.526 ± 17.947	0.92	14
ScoPMS 17	15 57 34.30	−23 21 12.2	M0V	−13.34 ± 0.12	−23.16 ± 0.08	US	144.216 ± 1.412	0.74	14
1RXS J155734.4-232112	15 57 34.30	−23 21 12.2	M1V	−13.34 ± 0.12	−23.16 ± 0.08	US	144.216 ± 1.412	1.25	14
HIP 78168	15 57 40.46	−20 58 59.0	B3V	−10.12 ± 0.18	−21.75 ± 0.12	US	156.379 ± 2.555	0.96	14
HIP 78196	15 57 59.34	−31 43 44.1	A0V	−13.79 ± 0.13	−26.10 ± 0.08	US	144.052 ± 1.236	0.01	14
HIP 78207	15 58 11.37	−14 16 45.6	B8Ia/Iab	−14.91 ± 0.49	−16.41 ± 0.38	US	133.026 ± 4.485	0.01	14
HD 142987	15 58 20.55	−18 37 25.1	G4	−16.78 ± 0.20	−22.67 ± 0.11	US	143.039 ± 1.894	0.40	14
HIP 78246	15 58 34.86	−24 49 53.3	B5V	−12.35 ± 0.30	−24.80 ± 0.16	US	146.171 ± 4.375	1.26	14
1RXS J155848.4-175758	15 58 47.72	−17 57 59.6	K3	−13.49 ± 0.10	−21.39 ± 0.05	US	138.973 ± 0.984	1.10	14
[PBB2002] USco J15591	15 59 18.39	−22 10 43.0	M4	−11.78 ± 0.27	−23.19 ± 0.15	US	147.655 ± 2.716	2.06	14
2MASS J16004056-2200322	16 00 40.56	−22 00 32.2	K7	−10.68 ± 0.09	−21.24 ± 0.04	US	153.066 ± 1.138	1.11	14
1RXS J160042.0-212730	16 00 42.76	−21 27 38.0	K7	−16.97 ± 0.46	−26.70 ± 0.34	US	159.022 ± 5.581	1.32	14
1RXS J160108.6-211320	16 01 08.01	−21 13 18.5	M0	−12.03 ± 0.08	−22.65 ± 0.05	US	147.492 ± 0.946	1.86	14
HIP 78483	16 01 18.42	−26 52 21.4	G0V	−16.65 ± 0.43	−25.07 ± 0.31	US	130.847 ± 4.203	1.70	14
ScoPMS 21	16 01 25.63	−22 40 40.2	K1IV	−12.14 ± 0.12	−23.60 ± 0.06	US	139.326 ± 1.228	1.20	14
HIP 78530	16 01 55.45	−21 58 49.3	B9V	−12.01 ± 0.12	−24.11 ± 0.07	US	137.272 ± 1.477	1.50	14
1RXS J160200.7-222133	16 02 00.39	−22 21 23.8	M1	−11.74 ± 0.13	−23.82 ± 0.06	US	144.548 ± 2.467	1.10	14
HIP 78549	16 02 13.55	−22 41 15.2	B9.5V	−12.51 ± 0.11	−23.53 ± 0.05	US	145.534 ± 1.588	2.13	14
[PGZ2001] J160222.4-1	16 02 22.48	−19 56 53.9	M3	−10.27 ± 0.21	−21.91 ± 0.09	US	155.438 ± 2.133	1.18	14
1RXS J160239.3-254157	16 02 39.10	−25 42 07.8	K7	−19.82 ± 0.09	−32.53 ± 0.05	US	113.149 ± 0.699	1.35	14
1RXS J160251.5-240204	16 02 51.22	−24 01 57.4	K4	−11.85 ± 0.11	−24.03 ± 0.05	US	143.918 ± 1.369	1.40	14
[PGZ2001] J160341.8-2	16 03 41.87	−20 05 57.7	M2	−10.69 ± 0.13	−22.15 ± 0.06	US	150.024 ± 1.424	0.51	14
1RXS J160355.8-203138	16 03 54.96	−20 31 38.5	M0	−10.51 ± 0.33	−21.64 ± 0.22	US	151.623 ± 5.089	1.86	14
[PZ99] J160357.6-2031	16 03 57.67	−20 31 05.6	K5	−11.60 ± 0.07	−22.90 ± 0.04	US	142.578 ± 0.782	1.10	14
HIP 78702	16 04 00.23	−19 46 02.9	B9.5V	−9.89 ± 0.12	−21.47 ± 0.05	US	152.518 ± 1.737	9.00	14
RX J1604.3-2130	16 04 21.66	−21 30 28.3	K2	−12.33 ± 0.10	−23.83 ± 0.04	US	150.116 ± 1.273	1.11	14
ScoPMS 27	16 04 47.75	−19 30 22.9	K2IV	−11.19 ± 0.15	−21.52 ± 0.07	US	146.657 ± 1.757	0.65	14
[PGZ2001] J160502.1-2	16 05 02.13	−20 35 07.1	M2	−9.95 ± 0.16	−22.04 ± 0.08	US	154.528 ± 1.790	1.50	14

Table 4
(Continued)

Name	RA (J2000.0)	DEC (J2000.0)	SpT	$\mu_\alpha \cos\delta$ (mas/yr)	μ_δ (mas/yr)	Association	Distance (pc)	Masses ($M_\odot$)	Surveys
ScoPMS 29	16 05 42.67	−20 04 15.2	M2V	−11.39 ± 0.58	−20.64 ± 0.31	US	110.570 ± 4.033	0.06	14
HIP 78847	16 05 43.38	−21 50 19.5	A0V	−10.97 ± 0.16	−30.89 ± 0.07	US	138.348 ± 1.992	0.89	14
/PGZ2001/ J160545.4-2	16 05 45.40	−20 23 08.8	M2	−11.02 ± 0.20	−22.98 ± 0.10	US	145.099 ± 2.155	0.07	14
1RXS J160612.4-203655	16 06 12.54	−20 36 47.2	K5	−10.55 ± 0.11	−22.94 ± 0.05	US	142.553 ± 0.918	0.64	14
/PGZ2001/ J160643.8-1	16 06 43.85	−19 08 05.5	K6	−7.06 ± 0.64	−19.21 ± 0.47	US	144.239 ± 6.659	2.13	14
HIP 78933	16 06 48.42	−20 40 09.1	B1V	−7.91 ± 0.81	−21.05 ± 0.68	US	141.651 ± 7.975	2.13	14
1RXS J160652.6-241627	16 06 54.36	−24 16 10.7	M3	−13.48 ± 0.10	−25.72 ± 0.05	US	151.416 ± 1.439	1.25	14
HIP 78956	16 07 04.67	−16 56 35.7	B9.5V	−10.65 ± 0.17	−20.32 ± 0.10	US	146.348 ± 1.809	2.06	14
/PGZ2001/ J160707.7-1	16 07 07.67	−19 27 16.2	M2	−10.55 ± 0.27	−20.65 ± 0.18	US	150.489 ± 3.061	0.16	14
/PGZ2001/ J160739.4-1	16 07 39.40	−19 17 47.2	M2	−9.12 ± 0.13	−24.04 ± 0.09	US	137.349 ± 1.245	0.27	14
1RXS J160814.2-190845	16 08 14.74	−19 08 32.6	K2	−8.53 ± 0.08	−29.38 ± 0.06	US	143.645 ± 1.318	2.70	14
/PGZ2001/ J160823.5-1	16 08 23.56	−19 11 31.6	M2	−9.17 ± 0.18	−24.76 ± 0.11	US	135.328 ± 1.717	0.13	14
1RXS J160831.4-180253	16 08 31.37	−18 02 41.4	M0	−8.79 ± 0.09	−23.38 ± 0.06	US	143.928 ± 0.872	1.22	14
/PZ99/ J160856.7-2033	16 08 56.72	−20 33 45.8	K5	−9.00 ± 0.12	−25.06 ± 0.07	US	143.988 ± 1.115	2.06	14
HIP 79124	16 09 02.60	−18 59 44.0	A0V	−7.76 ± 0.12	−24.15 ± 0.08	US	137.023 ± 1.244	2.00	14
HIP 79156	16 09 20.88	−19 27 25.9	A0V	−7.79 ± 0.13	−23.42 ± 0.09	US	150.597 ± 1.796	1.05	14
1RXS J160929.1-210524	16 09 30.30	−21 04 58.9	K7	−10.27 ± 0.11	−23.20 ± 0.08	US	139.674 ± 1.318	1.90	14
/PGZ2001/ J160933.8-1	16 09 33.79	−19 04 56.1	M2	−10.10 ± 0.11	−24.14 ± 0.07	US	137.464 ± 1.122	2.06	14
/PGZ2001/ J160954.4-1	16 09 54.41	−19 06 55.0	M2	−12.61 ± 0.12	−22.88 ± 0.07	US	136.832 ± 1.112	0.30	14
/PGZ2001/ J160959.4-1	16 09 59.33	−18 00 09.0	M4	−9.51 ± 0.21	−24.10 ± 0.13	US	136.226 ± 2.243	0.71	14
/PBB2002/ USco J16101	16 10 11.00	−19 46 03.9	M5	−11.60 ± 0.26	−22.94 ± 0.17	US	142.842 ± 3.895	0.53	14
HIP 79250	16 10 25.35	−23 06 23.3	A3III/IV	−18.74 ± 0.15	−30.62 ± 0.10	US	120.853 ± 1.275	0.31	14
/PGZ2001/ J161031.9-1	16 10 31.95	−19 13 06.0	K7	−9.34 ± 0.20	−23.59 ± 0.11	US	133.404 ± 1.277	0.07	14
/PBB2002/ USco J16105	16 10 52.41	−19 37 34.3	M1	−8.33 ± 0.22	−23.87 ± 0.15	US	144.822 ± 2.718	0.67	14
/PGZ2001/ J161115.3-1	16 11 15.34	−17 57 21.4	M1	−9.11 ± 0.12	−24.74 ± 0.08	US	136.505 ± 1.147	0.77	14
/PGZ2001/ J161118.1-1	16 11 18.13	−17 57 28.7	M4	−7.53 ± 0.49	−23.66 ± 0.36	US	147.992 ± 5.812	0.80	14
ScoPMS 45	16 11 20.57	−18 20 55.0	K5IVv	−8.95 ± 0.10	−24.66 ± 0.07	US	136.496 ± 1.183	1.10	13
HIP 79374	16 11 59.73	−19 27 38.5	B2IV	−6.86 ± 0.63	−28.25 ± 0.48	US	135.969 ± 6.455	1.58	13
HIP 79404	16 12 18.20	−27 55 34.9	B2V	−11.81 ± 0.81	−23.75 ± 0.67	US	150.346 ± 8.126	1.57	13
1RXS J161303.8-225745	16 13 02.71	−22 57 44.4	K4	−9.02 ± 0.09	−25.17 ± 0.07	US	140.109 ± 0.948	2.20	13
1RXS J161318.0-221251	16 13 18.58	−22 12 49.0	G9	−9.60 ± 0.14	−24.33 ± 0.10	US	134.329 ± 1.782	2.50	13
1RXS J161329.9-231122	16 13 29.28	−23 11 07.5	K1	−8.88 ± 0.09	−25.41 ± 0.07	US	138.748 ± 0.845	1.90	13
HIP 79530	16 13 45.49	−24 25 19.5	B6IV	−9.87 ± 0.25	−19.29 ± 0.17	US	167.154 ± 3.665	9.00	13
RX J1614.3-1906	16 14 20.28	−19 06 48.0	K5	−7.16 ± 0.22	−26.40 ± 0.15	US	142.965 ± 2.520	6.80	13
HIP 79643	16 15 09.27	−23 45 35.0	F2	−8.15 ± 0.08	−23.47 ± 0.06	US	154.480 ± 0.997	5.00	13
HIP 79797	16 17 05.40	−67 56 28.5	A4V	−45.99 ± 0.28	−84.00 ± 0.35	ARG	52.219 ± 1.145	7.80	13
HIP 79881	16 18 17.90	−28 36 50.5	A0V	−31.19 ± 0.26	−100.92 ± 0.18	BPIC	41.288 ± 0.375	3.50	13
PPM 747651	16 19 50.57	−33 54 45.3	G3	−17.42 ± 0.11	−25.47 ± 0.08	US	137.708 ± 0.997	7.80	13
HIP 80059	16 20 28.12	−21 30 32.4	A7III/IV	−12.24 ± 0.16	−25.92 ± 0.10	US	129.920 ± 1.520	7.00	13
HD 147491	16 23 22.92	−26 22 16.3	G2IV	−17.90 ± 0.09	−35.22 ± 0.06	US	107.956 ± 0.349	2.20	13
HIP 80311	16 23 47.17	−26 16 15.7	A0V	−9.76 ± 0.09	−20.82 ± 0.07	US	158.871 ± 1.246	3.25	13
HIP 81084	16 33 41.59	−09 33 11.9	M0.5V	−64.89 ± 0.07	−177.86 ± 0.10	ABD	31.087 ± 0.034	5.00	13
HIP 81266	16 35 52.95	−28 12 57.7	B0V	−7.64 ± 1.97	−17.94 ± 2.00	US	195.190 ± 42.290	1.62	13
HIP 82319	16 49 12.21	−22 42 41.6	F3V	−6.56 ± 0.08	−22.37 ± 0.04	US	140.475 ± 0.801	2.50	13
HIP 82688	16 54 08.14	−04 20 24.7	G0V	−37.25 ± 1.01	−114.05 ± 0.73	ABD	46.728 ± 2.008	2.50	13
HIP 83494	17 03 53.58	34 47 24.8	A5V	−60.92 ± 0.26	−5.05 ± 0.34	THA	54.975 ± 0.936	2.50	13

Table 4
(Continued)

Name	RA (J2000.0)	DEC (J2000.0)	SpT	$\mu_\alpha \cos\delta$ (mas/yr)	μ_δ (mas/yr)	Association	Distance (pc)	Masses ($M_\odot$)	Surveys
HIP 84586	17 17 25.51	−66 57 03.7	G5IV	−21.83 ± 0.39	−136.91 ± 0.42	BPIC	31.446 ± 0.494	2.20	13
HD 155555 C	17 17 31.27	−66 57 05.4	M3Ve	−14.75 ± 0.06	−145.10 ± 0.09	BPIC	71.911 ± 0.698	10.00	13
HIP 84642	17 18 14.65	−60 27 27.5	G8V	−54.62 ± 1.09	−91.04 ± 0.84	THA	58.927 ± 4.653	2.50	13
CD-54 7336	17 29 55.05	−54 15 48.6	K1V	−5.41 ± 0.06	−63.54 ± 0.06	BPIC	104.679 ± 0.865	2.20	13
HIP 86346	17 38 39.63	61 14 16.0	M0V	−23.30 ± 2.03	47.71 ± 2.20	ABD	33.123 ± 2.194	2.20	13
HD 164249 A	18 03 03.40	−51 38 56.4	F5V	2.34 ± 0.07	−86.09 ± 0.07	BPIC	49.615 ± 0.123	2.00	13
HR 6750	18 06 49.90	−43 25 30.8	A5V	10.73 ± 1.05	−106.59 ± 0.51	BPIC	41.841 ± 1.155	7.80	13
HD 168210	18 19 52.19	−29 16 32.8	G5V	4.38 ± 0.09	−46.19 ± 0.08	BPIC	104.679 ± 0.865	7.80	13
2MASS J18420694-5554254	18 42 06.93	−55 54 25.4	M3.5	9.70 ± 12.10	−81.20 ± 2.80	BPIC	94.795 ± 0.260	4.00	13
HIP 92024 A	18 45 26.87	−64 52 16.5	A7	32.07 ± 0.25	−150.18 ± 0.31	BPIC	28.337 ± 0.183	1.70	13
HIP 92024 BC	18 45 37.00	−64 51 46.1	K7V	17.16 ± 0.07	−155.06 ± 0.09	BPIC	94.795 ± 0.260	1.90	13
CD-31 16041	18 50 44.47	−31 47 47.4	K7Ve	17.37 ± 0.07	−72.27 ± 0.05	BPIC	94.795 ± 0.260	2.20	13
HIP 92680	18 53 05.85	−50 10 49.8	G9IV	16.34 ± 0.08	−85.25 ± 0.08	BPIC	47.127 ± 0.133	16.00	13
HR 7214	19 03 32.23	01 49 07.5	A4V	17.67 ± 0.23	−65.29 ± 0.19	ABD	38.560 ± 0.048	1.69	13
HIP 94235	19 10 57.85	−60 16 19.9	G1V	12.51 ± 0.79	−100.15 ± 0.68	ABD	61.349 ± 2.898	1.58	13
Eta Tel A	19 22 51.21	−54 25 26.2	A0V	25.57 ± 0.21	−82.71 ± 0.14	BPIC	48.216 ± 0.488	0.89	13
HIP 95270	19 22 58.94	−54 32 16.9	F5.5	24.56 ± 0.07	−81.91 ± 0.04	BPIC	99.571 ± 0.386	1.52	3,13
Rukbat	19 23 53.15	−40 36 57.3	B8	31.36 ± 0.76	−119.32 ± 0.78	ABD	54.404 ± 1.411	0.59	13
UCAC3 116-474938	19 56 03.88	−32 07 37.6	M4	35.20 ± 1.80	−59.90 ± 1.50	BPIC	99.571 ± 0.386	0.98	13
eps Pav	20 00 35.54	−72 54 37.8	A0	79.91 ± 0.53	−131.70 ± 0.56	ARG	31.380 ± 0.322	1.45	13
DENIS J200048.3-752306	20 00 48.40	−75 23 07.0	M9	69.00 ± 12.00	−110.00 ± 4.00	BPIC	130.412 ± 0.629	1.40	13
HIP 99273	20 09 05.20	−26 13 26.5	F5V	40.16 ± 0.07	−67.38 ± 0.05	BPIC	50.135 ± 0.108	0.63	13
2MASS J20100002-2801410	20 10 00.03	−28 01 41.0	M3V	40.70 ± 3.00	−62.00 ± 1.70	BPIC	47.961 ± 3.059	1.10	13
HIP 99770	20 14 32.03	36 48 22.5	A2V	69.81 ± 0.19	69.14 ± 0.20	ARG	42.698 ± 0.401	1.30	13
HIP 100751	20 25 38.86	−56 44 06.3	B2IV	6.90 ± 0.44	−86.02 ± 0.32	THA	54.824 ± 1.562	0.97	13
1SWASP J203337.61-255651.	20 33 37.58	−25 56 52.1	M4.5	52.80 ± 1.70	−75.90 ± 1.30	BPIC	101.081 ± 0.378	1.18	13
AT Mic B	20 41 51.14	−32 26 10.2	M4Ve	297.09 ± 0.13	−302.75 ± 0.10	BPIC	67.755 ± 0.165	0.98	13
AT Mic A	20 41 51.14	−32 26 06.5	M4Ve	247.20 ± 0.11	−415.56 ± 0.08	BPIC	9.881 ± 0.007	1.30	13
2MASS J20434114-2433534	20 43 41.14	−24 33 53.1	M4.1V+M3.7V	62.00 ± 10.00	−60.00 ± 10.00	BPIC	35.587 ± 4.939	0.53	13
HIP 102409	20 45 09.53	−31 20 27.2	M1V	279.96 ± 1.26	−360.61 ± 0.73	BPIC	9.909 ± 0.104	0.89	13
HIP 103311	20 55 47.67	−17 06 51.0	F8V	58.81 ± 0.83	−62.83 ± 0.73	BPIC	45.662 ± 1.605	1.08	13
2MASS J21100535-1919573	21 10 05.35	−19 19 57.3	M2	89.00 ± 0.90	−89.90 ± 1.80	BPIC	79.383 ± 0.333	1.02	13
HIP 105388	21 20 49.96	−53 02 03.1	G7V	28.77 ± 1.01	−94.19 ± 0.55	THA	42.973 ± 1.809	0.37	13
BS Ind	21 20 59.78	−52 28 40.0	G9V(e)	30.62 ± 0.55	−95.91 ± 0.52	THA	52.667 ± 0.918	0.89	13
LQ Peg	21 31 01.70	23 20 07.3	K8V	134.53 ± 0.06	−144.67 ± 0.07	ABD	79.383 ± 0.333	1.25	13
HIP 107345	21 44 30.12	−60 58 38.9	M1V	39.98 ± 2.35	−91.66 ± 1.56	THA	43.649 ± 4.915	0.78	13
HN Peg	21 44 31.31	14 46 18.9	G0V	231.08 ± 0.10	−113.13 ± 0.09	HLY	39.764 ± 0.040	1.14	13
HIP 107947	21 52 09.71	−62 03 08.5	F6V	44.02 ± 0.04	−91.09 ± 0.06	THA	47.038 ± 0.079	1.10	13
TYC 5899-0026-1	21 52 10.42	05 37 35.9	M3V	105.70 ± 1.50	−147.40 ± 1.40	ABD	30.497 ± 5.254	1.40	13
HIP 108195 A	21 55 11.37	−61 53 11.7	F3	42.80 ± 0.59	−89.67 ± 0.57	THA	54.259 ± 1.215	0.83	13
HIP 108422	21 55 11.39	−61 53 11.8	F3V	44.50 ± 0.23	−91.07 ± 0.27	THA	46.468 ± 0.885	0.38	13
2MASS J22021626-4210329	22 02 16.24	−42 10 32.9	M1	50.40 ± 1.00	−90.90 ± 1.50	BPIC	51.355 ± 0.131	1.10	13
HIP 109268	22 08 13.98	−46 57 39.5	B6V	126.69 ± 0.14	−147.47 ± 0.14	ABD	30.969 ± 0.201	1.00	13
1RXS J221419.3+253411	22 14 17.66	25 34 06.6	M4.3V	164.00 ± 5.00	−44.00 ± 5.00	COL	28.735 ± 2.064	1.06	13
HIP 110526	22 23 29.11	32 27 34.1	M3V	255.30 ± 3.10	−207.80 ± 2.90	ABD	15.511 ± 1.561	0.67	13
HIP 112312	22 44 57.97	−33 15 01.7	M4IV	184.76 ± 2.64	−119.76 ± 2.31	BPIC	23.342 ± 1.967	0.54	13
HIP 113579	23 00 19.82	−26 09 13.5	G5V	113.54 ± 2.13	−162.04 ± 1.52	ABD	30.543 ± 1.893	1.40	13

Table 4
(Continued)

Name	RA (J2000.0)	DEC (J2000.0)	SpT	$\mu_\alpha \cos\delta$ (mas/yr)	μ_δ (mas/yr)	Association	Distance (pc)	Masses ($M_\odot$)	Surveys
HIP 114066	23 06 04.84	63 55 34.4	M1V	171.46 ± 1.59	−58.55 ± 1.57	ABD	24.503 ± 0.960	0.49	13
HR 8799	23 07 28.70	21 08 03.3	A5	108.30 ± 0.16	−49.48 ± 0.15	COL	41.291 ± 0.150	1.00	13
HIP 114530	23 11 52.05	−45 08 10.6	G5V	87.53 ± 1.39	−93.36 ± 0.79	ABD	50.761 ± 2.834	1.10	13
2MASS J23131671-4933154	23 13 16.70	−49 33 15.4	M4	77.50 ± 2.10	−88.10 ± 1.70	BPIC	28.679 ± 0.060	0.89	13
HIP 115162	23 19 39.56	42 15 09.8	G4V	77.52 ± 0.73	−66.90 ± 0.96	ABD	50.150 ± 2.867	0.52	13
HD 220825	23 26 55.94	01 15 20.1	A0	87.11 ± 0.34	−95.72 ± 0.28	ABD	48.918 ± 0.516	0.63	13
2MASS J23285763-6802338	23 28 57.62	−68 02 33.8	M2.5	66.80 ± 1.90	−67.10 ± 1.70	BPIC	49.615 ± 0.083	0.39	13
G190-27	23 29 22.58	41 27 52.2	M4.2V	415.00 ± 7.50	−41.00 ± 6.70	COL	14.792 ± 0.393	0.19	13
2MASS J23320018-3917368	23 32 00.16	−39 17 36.8	M3	193.40 ± 17.90	−178.40 ± 17.90	BPIC	56.110 ± 0.415	0.89	13
HIP 116748 A	23 39 39.47	−69 11 44.6	G5V	79.46 ± 0.07	−67.44 ± 0.04	THA	44.118 ± 0.068	0.32	13
HIP 116805	23 40 24.49	44 20 02.1	B9V	80.73 ± 0.14	−18.70 ± 0.15	COL	51.626 ± 0.506	0.80	13
HD 222575	23 41 54.28	−35 58 39.8	G8V	71.34 ± 0.12	−66.06 ± 0.06	ABD	64.666 ± 0.200	0.83	13
2MASS J23452225-7126505	23 45 22.25	−71 26 50.5	M3.5	80.30 ± 2.20	−62.40 ± 2.10	BPIC	48.213 ± 0.134	1.25	13
2MASS J23474694-6517249	23 47 46.94	−65 17 24.9	M1.5	79.20 ± 1.20	−66.80 ± 1.20	BPIC	48.213 ± 0.134	1.51	13
HD 223352 AB	23 48 55.53	−28 07 48.9	A0V	100.11 ± 0.67	−104.68 ± 0.64	ABD	42.744 ± 0.712	1.45	13
HIP 118121	23 57 35.06	−64 17 53.6	A1V	78.85 ± 0.65	−62.04 ± 0.61	THA	47.074 ± 0.806	10.00	13

or if $\alpha \neq -1$ and $\beta = -1$

$$n_{i,j} = \frac{f}{D}[M_{i+1}^{\alpha} - M_i^{\alpha}] \ln\left(\frac{a_{i+1}}{a_i}\right), \quad (9)$$

or if $\alpha = -1$ and $\beta \neq -1$

$$n_{i,j} = \frac{f}{D} \ln\left(\frac{M_{i+1}}{M_i}\right)[a_{i+1}^{\beta} - a_i^{\beta}], \quad (10)$$

where $D = (M_{\max}^{\alpha+1} - M_{\min}^{\alpha+1})(a_{\max}^{\beta+1} - a_{\min}^{\beta+1})$.

The number of companions expected in a bin (i, s), of given mass and projected separation, is equal to the number of companions expected in bin (i, j), of mass and semimajor axis, multiplied by the probability $p(s|j)$ of the companions to be observed at projected separation s given their semimajor axis j, and summed up over all semimajor axis bins,

$$n_{is} = \sum_j n_{ij} p(s|j). \quad (11)$$

The probability $p(s|j)$ is computed using a Monte Carlo simulation assuming the same eccentricity distribution as before and accounting for random orientations and phases of the observations. Factoring in the completeness of the observations, the expected number of detected planets in bin (i, s) for star k is thus $C_{k,is}n_{is}$. Assuming that the presence of a planet in a given bin does not depend on the presence of other planets in other bins and using Poisson statistics for each bin and each star, we have that the probability P of obtaining the observed results in a given bin given the assumed models is given by

$$P(\{d_{k,is}\}|\{\alpha, \beta, f\}) = e^{-C_{k,is}n_{is}}(C_{k,is}n_{is})^{d_{k,is}}. \quad (12)$$

Thus, the likelihood of the whole survey results is obtained by multiplying the above probability for all bins and all stars:

$$\mathcal{L}(\{d_{k,is}\}|\{\alpha, \beta, f\}) = \prod_{k=1}^{N} \prod_{i,s} e^{-C_{k,is}n_{is}}(C_{k,is}n_{is})^{d_{k,is}}, \quad (13)$$

or

$$\ln \mathcal{L} = \sum_{i,j,k} \ln[(C_{k,is}n_{is})^{d_{k,is}}] - C_{k,is}n_{is}. \quad (14)$$

This is the form we used in the calculations that follow. The set $\{d_{k,is}\}$ for our survey includes the detection of seven companions, as mentioned in Section 2. In this section, we consider the full range of separations from 5 to 5000 au, rather than only 20–5000 au as in the previous analysis; a justification will be provided later.

To constrain the parameters α, β, and f that define the companion distribution, we used the *emcee* (Foreman-Mackey et al. 2013) Python implementation of the affine-invariant MCMC ensemble sampler of Goodman & Weare (2010). The MCMC sampler iteratively generates, for each of several random walkers, a sequence of samples for the three parameters in our model. We used uniform priors on all parameters (in log scale for f) and we defined the starting parameter values for the walkers to be drawn randomly from a uniform distribution between -3 and 1 for $\log f$, between -4.9 and 4.9 for α, and between -4.9 and 4.9 for β. We discarded the first 25% of the steps as the burn-in phase and considered that the remaining samples were representative of the posterior densities. The likelihood function is computed at each iteration, for each set of parameters. At each step, the sampler tries to move the walkers randomly in the parameter space: if the new set of parameters corresponds to a higher probability density part of the posterior distribution, then the move is accepted, otherwise, the new set can be accepted or rejected depending on the trial positions. The sampler thus mostly probes the higher probability region of the parameter space and the final output samples are representative of the posterior distributions for each parameter of the model.

Figure 5 shows the results for 200 walkers and 1000 steps. The results indicate that $\alpha = -0.08^{+0.75}_{-0.63}$, $\beta = -1.41^{+0.22}_{-0.24}$, and $f = 0.12^{+0.11}_{-0.06}$, where the uncertainty corresponds to 68% confidence intervals. This indicates an increased planet occurrence for smaller semimajor axes, while the planet mass distribution shows a marginal decrease with mass. The parameters α and β show no correlation between each other.

Results from RV surveys have shown that the host star mass is correlated with the presence of planets (Johnson et al. 2010). In the case of planets on wide orbits, there seems to be no significant trend in planet frequency with host mass (Bowler 2016) or a moderate trend (Lannier et al. 2016) that would indicate that planets on wide orbits may be more common around more massive stars. To investigate this, we added a dependence on the host star mass in the distribution of planets. The planet distribution then becomes

$$d^2n = f\frac{\alpha\beta}{C}\left(\frac{M_\star}{M_\odot}\right)^{\gamma} M^{\alpha}a^{\beta}dMda. \quad (15)$$

The mass of each star in the sample was estimated from either its spectral type or its J-band absolute magnitude. For stars with spectral types from late-B to late-K, we used the evolution models of Siess et al. (2000) to estimate the mass from the spectral type and the age. For stars with spectral types of M0 or later, we used models from Baraffe et al. (2015) to estimate the mass from the J-band magnitude and the age. The masses for the earlier-type stars (<late-B) were taken from Lafrenière et al. (2014), where they were estimated using the evolution models of Schaller et al. (1992). Lastly, the mass of HIP 100751 was taken from David & Hillenbrand (2015).

This new model has four parameters. In our MCMC, we used the same initial ranges for our walkers for the three parameters we had previously, and for γ we used random values in the range of -4.9 to 4.9. We used uniform priors on all parameters, 200 walkers and 1000 steps. The results are shown on Figure 6. No correlation is seen between α and β, γ and β, or α and γ. However, the frequency f is correlated to all other parameters. Our results indicate that the best parameter values are $\alpha = -0.18^{+0.77}_{-0.65}$, $\beta = -1.43^{+0.23}_{-0.24}$, $\gamma = 0.62^{+0.56}_{-0.50}$, and $f = 0.11^{+0.11}_{-0.05}$. The values for α, β and f are consistent within uncertainties to the values obtained with the previous models. The added parameter γ shows that the number of planets is correlated with the host star mass, such that massive stars host more planets in the separation and mass domains considered here.

As mentioned above, in this section we considered the full range from 5 to 5000 au instead of the 20–5000 range used in Section 3.1. To verify our choice of orbital separation range, we repeated the calculations in this section but over the 20–5000 au range, and in the case where the distribution is described by Equation (6), we obtained $\alpha = -0.10^{+0.75}_{-0.65}$, $\beta = -1.58^{+0.29}_{-0.26}$, and $f = 0.23^{+0.35}_{-0.15}$. Thus, both semimajor axis intervals favor similar α and β, but the overall planet frequency is significantly higher

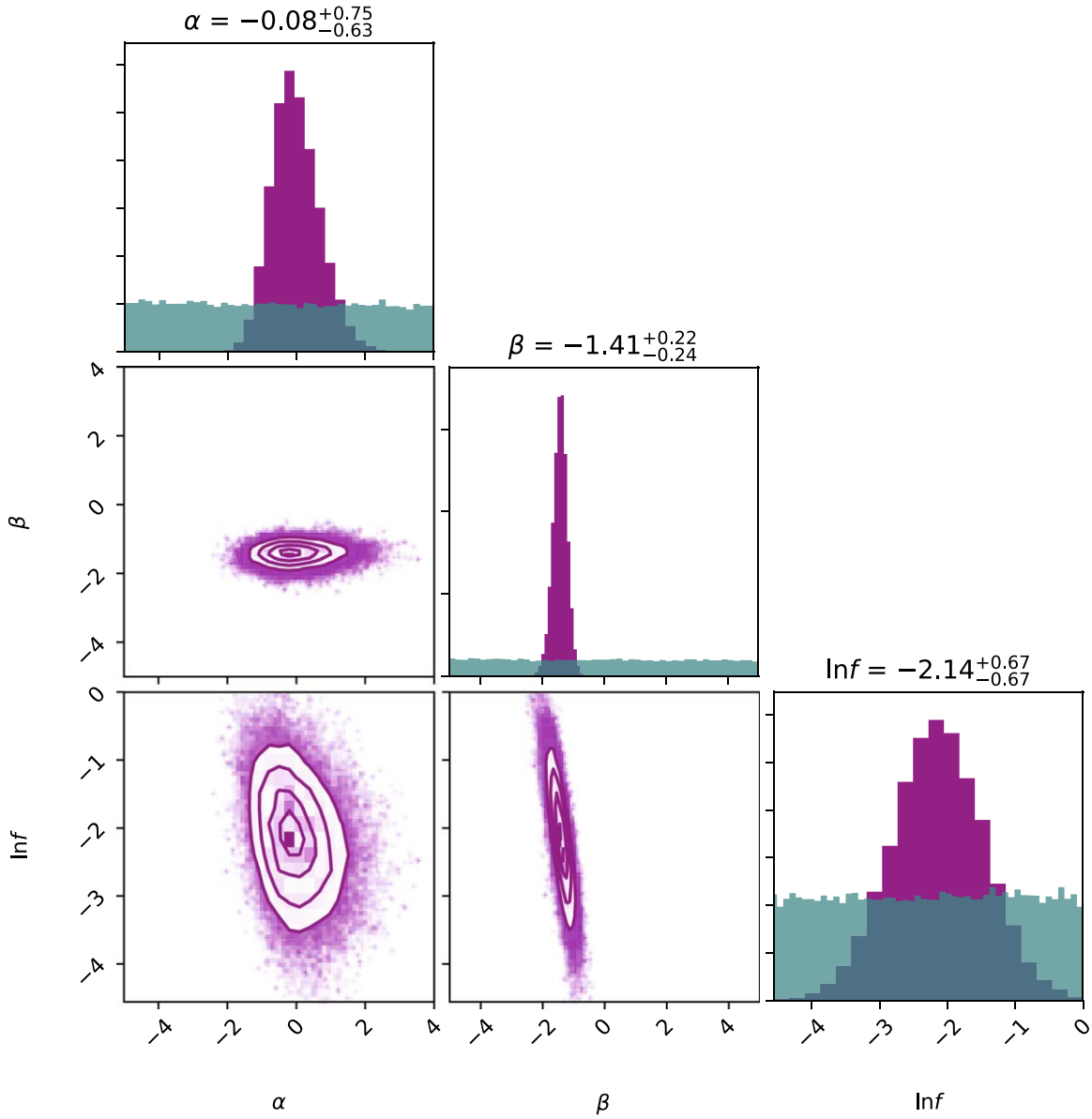

Figure 5. Results of the MCMC simulations for all the stars of the sample. The histogram represent the marginalized posterior probability distributions for our three parameters: α, β, and f. Correlation plots for the parameters are also shown, with the solid contour lines corresponding to regions containing 68%, 95%, and 99% of the posterior. We use 200 walkers with 1000 steps. Here, purple indicates the highest values of the likelihoods and whites indicates the lowest. The posterior distributions of the priors are also shown in teal in the histograms, for reference.

and has much larger uncertainties for the 20–5000 au interval (although both agree within uncertainties). The higher uncertainty on the frequency for the 20–5000 au range can be understood on the basis of the favored slope of the semimajor axes distribution, which puts much more planets on shorter orbits. The effect of a change in planet frequency is thus more pronounced at the shortest separations, and neglecting the observational information that we have in the 5–20 au interval, even if incomplete, has a big impact on the frequency uncertainty. For the analyses in this section, we decided to keep the range that provides the lowest uncertainties, namely the 5–5000 au interval.

3.3. Comparison with Cold-start Models

The analysis described in the earlier sections uses hot-start models. However, it is possible that planets on wide orbits formed through a cold-start. For planets at more than hundreds of astronomical unit separations, this would likely mean that they formed in the disk at smaller separations and migrated out. In the cold-start models, an accretion shock is created by free-falling gas onto the protoplanet, which irradiates the gravitational potential energy away from the core. This leaves newly formed planets with low entropies and luminosities. Young massive planets are much fainter in cold-start models than in hot-start models. This effect is particularly important for young objects as the luminosity for both hot- and cold-start models is similar at 200 Myr and beyond, as the initial condition effects are washed away by evolution.

To investigate the impact that a cold-start formation would have on our results, we did one more analysis similar to those presented in Section 3.1 but this time we used cold-start models from Fortney et al. (2008). The Fortney et al. (2008) models give $T_{\rm eff}$ and R for given masses as a function of age. To use

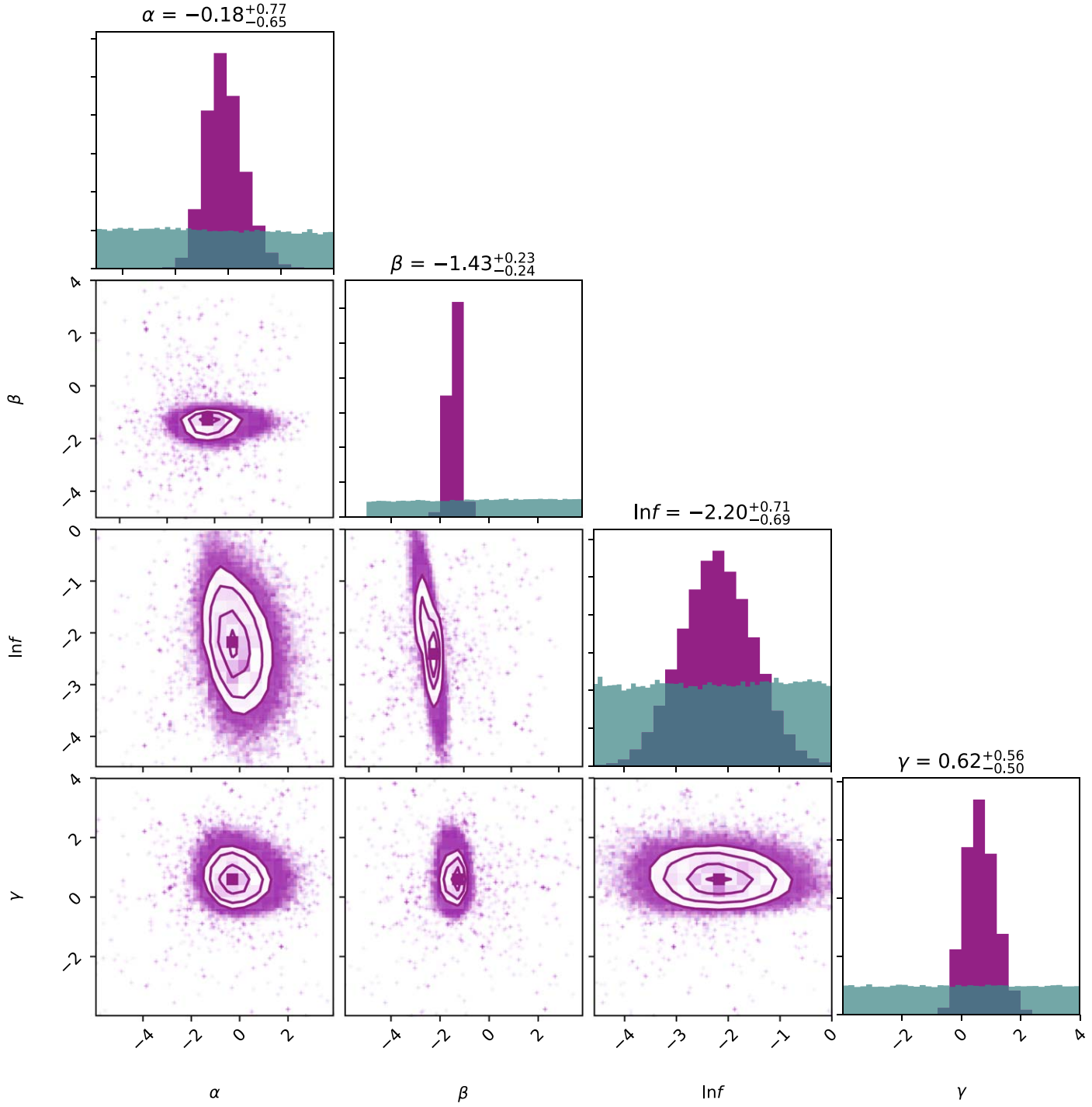

Figure 6. Same as Figure 5 but with four parameters and using the distribution of planets from Equation (15).

these models for our purpose, we first had to interpolate the given values at the ages of the stars in our sample and on our grid of masses; because the models were available only up to 10 $M_{\rm Jup}$, we linearly extrapolated the models from 10 to 20 $M_{\rm Jup}$ to complete our grid, neglecting luminosity bursts due to deuterium burning for objects more massive than 13 $M_{\rm Jup}$, and we calculated synthetic magnitudes for all filters used in our study. To do so, we used synthetic spectra from the BT-Settl atmospheric models, scaled to the luminosity of the models, in combination with the appropriate filter response functions. The synthetic spectra are only available for log $g = 4$ and effective temperatures ranging from 400 to 600 K; when the surface gravity of the models was below 4, we used a synthetic spectrum with log $g = 4$. Furthermore, the cold-start models yield planets with effective temperatures in the range of 170–560 K, extending much below the lowest temperature (400 K) of the synthetic spectra. The effective temperatures of the cold-start models in the range of 400–600 K were thus interpolated into the atmospheric grid at temperatures of 400, 500, or 600 K, and effective temperatures in 350–400 K were extrapolated, while temperatures below 350 K were considered too cold to be detected. We were then able to

calculate cold-start contrast maps for each star. The completeness maps for the cold-start models are not as good as for the hot-start models, since companions of mass 1–20 $M_{\rm Jup}$ are much fainter in the former models. Indeed, a 10 $M_{\rm Jup}$ can be 5 magnitudes fainter in cold-start models than in hot-start models. Still, with the cold-start completeness maps, we inferred the frequency of companions of masses between 1 and 20 $M_{\rm Jup}$ and separations of 5–5000 au as we did previously in Section 3.1. In the case of the cold-start models, the set $\{d_k\}$ is 0 for all targets, as all detected companions would be more massive than 20 $M_{\rm Jup}$ according to those models. We obtained an upper limit of 5.2%, at a 95% confidence level, for companions with masses in 1–20 $M_{\rm Jup}$ and separation in the 5–5000 au range, which is only slightly higher than the companion frequency inferred from the hot-start models.

4. Discussion

The frequency of Jupiter-like planets has been evaluated many times before from surveys made with techniques other than direct imaging. One study often quoted is that by Cumming et al. (2008) as mentioned in the introduction. Based on 8 yr of precise RV measurements from the Keck Planet Search, they inferred that 10.5% of solar-type stars have a companion with a mass of 0.3–10 $M_{\rm Jup}$ and a semimajor axis below 3 au. Similarly, based on the results of the High Accuracy Radial Velocity Planet Searcher (HARPS), Mayor et al. (2011) found that 9.7% ± 1.3% of stars host a gas giant ($>0.3\,M_{\rm Jup}$) with a semimajor axis <4.6 au. Taken at face values and in comparison with the RV results, our results indicate that giant planets are less frequent above 5 au than below, even when summing the planet population all the way up to 5000 au. One possible caveat here is that our imaging survey has very little sensitivity to planets below 1–2 $M_{\rm Jup}$, and thus that a population of low-mass giant planets may be unaccounted for in our results.

Estimates of giant planet occurrence were also derived from microlensing surveys. Based on the OGLE survey follow-up by the PLANET collaboration, Cassan et al. (2012) find that 17^{+6}_{-9}% of stars host massive planets (0.3–10 $M_{\rm Jup}$) with a semimajor axis between 0.5 and 10 au. This frequency is marginally higher than the one we infer here from direct imaging surveys, $2.61^{+6.97}_{-1.00}$% for the 20–5000 au range. If we assume that about 10% of the microlensing survey results are accounted for by planets below 5 au, per the above RV results, then the remainder would be in very good agreement with our results. In turn, this would indicate that within our range of sensitivity most of the planets at the larger separations would be located toward the small semimajor axes, which is indeed as we observed in our sample.

Another caveat to our results is that our mass determinations are indirect, relying on mostly uncalibrated evolution models. If young giant planets are much fainter than expected by hot-start models, then possibly much more than currently estimated could have been missed by the observations, leading to an underestimate of giant planet occurrence at large separations. Our results based on the cold-start models suggest that this is however not the case. Giant planets thus seem to be less frequent at large separations than small separations even when applying cold-start models.

It has often been assumed that the companion mass and semimajor axis distribution of the RV planets can be extrapolated for planets onto larger orbits, at least up to some point. Converting

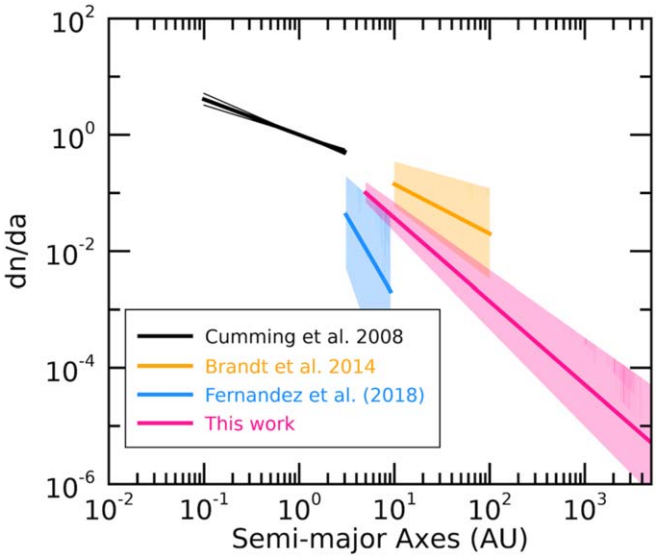

Figure 7. Comparison of the slopes of various power-law semimajor axis distributions of companions ($dn = a^{\beta}$). The RV distribution of planets from Cumming et al. (2008) is shown in black. The broken power-law distribution of transiting and RV planets from Fernandes et al. (2019) is drawn in blue; the turnover point is at 3 au. The direct imaging distribution of brown dwarfs from Brandt et al. (2014) is drawn in orange. Only the slopes are depicted here, and all curves are normalized at a semimajor axis of 1 au.

the Cumming et al. (2008) period distribution mentioned in the introduction into a semimajor axis power-law distribution, in line with Equation (6), yields a value of $\beta = -0.69 \pm 0.15$. This means that giant planets on short orbits are more common than on wide orbits. Our value for β of $-1.43^{+0.23}_{-0.24}$, which is significantly different from that of Cumming et al. (2008), possibly hints that the more massive planets (several $M_{\rm Jup}$ or more) on orbits $\gg$5 au probed here are part of a different population than the less massive RV planets at $\lesssim$3 au.

Figure 7 compares the slopes of various power-law distributions in planet semimajor axes found in the literature. The slopes obtained in this work are shown in pink and are compared with the slopes from RV planet distributions from Cumming et al. (2008) in black and Fernandes et al. (2019; asymmetrical distribution) in blue. The direct imaging distribution of brown dwarfs from Brandt et al. (2014) is drawn in orange. While the slope from Cumming et al. (2008) is not consistent with the one we measure, as noted earlier, the slope from Fernandes et al. (2019) at separations greater than the snow line is marginally consistent. The slope reported by Brandt et al. (2014) for more massive, 5–70 $M_{\rm Jup}$, companions is also marginally consistent with ours. Overall, we measure a sharp decrease with semimajor axis, which is broadly consistent with the distribution of planets with a semimajor axis greater than 3 au seen with RV and with brown dwarf companions to main-sequence stars.

Figure 8 compare the slopes of various power-law distributions in mass. Our results, shown in pink, are in good agreement with the slope of the mass distribution of brown dwarf companions from Metchev & Hillenbrand (2009) in green and Brandt et al. (2014) in orange. They also agree with the slope for stellar companions at larger separations from Duchêne & Kraus (2013), shown in navy blue. However, it is not in agreement with the slopes of the distributions of RV planets from Cumming et al. (2008) in black and Fernandes et al. (2019) in blue. This may

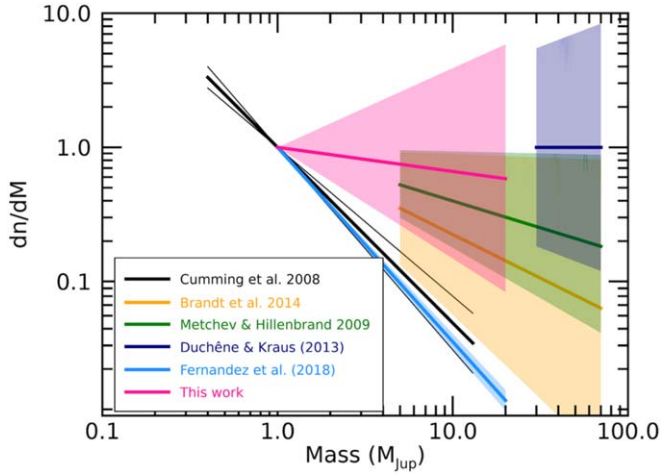

Figure 8. Comparison of the slopes of various power-law mass distributions of companions ($dn = M^{\alpha}$). The RV distribution of planets from Cumming et al. (2008) is shown in black and for Fernandes et al. (2019) it is shown in blue. The direct imaging distribution of brown dwarfs from Metchev & Hillenbrand (2009) is drawn in green and from Brandt et al. (2014) in orange. The distribution of stellar companions from Duchêne & Kraus (2013) is shown in navy blue. The distribution of companions from this work is drawn in pink. The slope our distribution is consistent with slopes from the distribution of brown dwarfs or stellar companions. Only the slopes are depicted here, and all curves are normalized at a mass of 1 $M_{\rm Jup}$.

suggest that our survey is probing the low-mass tail of the brown dwarf and stellar companion distribution rather than the continuation of the distribution of planets observed at smaller semimajor axes.

Vigan et al. (2017) compiled 12 direct imaging surveys and compared the results to models based on the gravitational instability formation scenario from Forgan & Rice (2013). In that study they showed that, assuming that companions form by the gravitational instability process, the models predict that the occurrence of companions increases with separation between 1 and 20 au but decreases slowly with separation beyond. This change in the distribution with the semimajor axis might be evidence for a change of populations where the closer planets would be a population of nonscattered planets while the planets on wide orbits would be coming from a population of scattered planets. Qualitatively, our results at large separations agree with the simulations as we find a number of companions that decreases with semimajor axes. However, our slope is steeper that the slopes presented in Vigan et al. (2017).

Surveys focusing on probing the binary fraction of stars of all spectral types tend to show that the binaries with a low-mass component decline in number and have closer separations (Raghavan et al. 2010). Also, binary fraction decreases with decreasing mass (Chabrier et al. 2005; Fontanive et al. 2018). Those results are consistent with our work, as our results show that companions are more frequent for more massive host stars.

5. Conclusions

We used an MCMC analysis to put constraints on the distribution of 1–20 $M_{\rm Jup}$ companions at separations of 5–5000 au from a compilation of direct imaging surveys using the DIVA archives, a survey of Upper Scorpius, the PSYM-WIDE survey, and the WEIRD survey. We used a distribution of planets in the form of a power law in mass and the semimajor axis of planets and host star mass. In general, we found that the occurrence of planets increases with smaller planet masses, closer orbits, and around more massive stars. Moreover, our constraints on the mass distribution shows that it is in better agreement with the mass distribution of brown dwarfs and stellar companions than it is with the distribution of planetary companions found by RV at smaller separations.

The constraints on the distribution of companions found in this work depend on and are limited by the number of planets that the sample holds. In particular, while a wide range of semimajor axis is covered by the seven planets, the range in mass is rather narrow, as all the planets have very similar masses. This prevents us from reaching strong constraints on the α parameter controlling the power-law distribution in planet mass. Thus, the search for planets using direct imaging should continue to uncover a larger and more diverse sample of planets enabling to better constrain their distribution.

In this work, we have chosen to fit our sample with a single power-law distribution. The next step in this project would be to use different distributions, for example a broken power law in planet mass. This particular distribution would be motivated for instance by the work from Santos et al. (2017) who have found evidence of a change in the population of giant planets at 4 $M_{\rm Jup}$. They suggest that the lower-mass planets are formed by the core accretion process, while the more massive planets are mainly formed through the gravitational instability scenario, with an overlap of the two processes at 4 $M_{\rm Jup}$. Also, Reggiani et al. (2016) suggested a superposition of two different populations to explain their null results from direct imaging. They coupled the brown dwarf companion distribution to the planet companion distribution truncated at about 100 au. This new distribution has a minimum for companion masses in 10–50 $M_{\rm Jup}$, which can explain the lack of objects in this range of masses without having to introduce another formation process for brown dwarfs. This is another distribution that could be investigated with our sample, or preferably, with an expanded sample containing more detected companions and spanning a wider range of companion masses.

The authors thank the anonymous referee for the constructive comments and suggestions that improved the overall quality of the paper.

This work was financially supported by the Natural Sciences and Engineering Research Council (NSERC) of Canada and the Fond de Recherche QuébécoisNature et Technologie (FRQNT; Québec).

This publication makes use of data products from the Two Micron All Sky Survey, which is a joint project of the University of Massachusetts and the Infrared Processing and Analysis Center, and funded by the National Aeronautics and Space Administration and the National Science Foundation, of the NASA Astrophysics Data System Bibliographic Services, the VizieR catalog access tool, and the SIMBAD database operated at CDS, Strasbourg, France.

This research has made use of the Direct Imaging Virtual Archive (DIVA), operated at CeSAM/LAM, Marseille, France.

This work has made use of data from the European Space Agency (ESA) mission *Gaia* (https://www.cosmos.esa.int/gaia), processed by the *Gaia* Data Processing and Analysis Consortium (DPAC, https://www.cosmos.esa.int/web/gaia/dpac/consortium). Funding for the DPAC has been provided by national institutions, in particular the institutions participating in the *Gaia* Multilateral Agreement.

Software: emcee.

ORCID iDs

Frédérique Baron https://orcid.org/0000-0002-5074-1128
David Lafrenière https://orcid.org/0000-0002-6780-4252
Étienne Artigau https://orcid.org/0000-0003-3506-5667
Jonathan Gagné https://orcid.org/0000-0002-2592-9612
Julien Rameau https://orcid.org/0000-0003-0029-0258
Marie-Eve Naud https://orcid.org/0000-0003-1807-1598

References

Allard, F., Hauschildt, P. H., Alexander, D. R., Tamanai, A., & Schweitzer, A. 2001, ApJ, 556, 357
Artigau, É., Gagné, J., Faherty, J., et al. 2015, ApJ, 806, 254
Baraffe, I., Chabrier, G., Barman, T. S., Allard, F., & Hauschildt, P. H. 2003, A&A, 402, 701
Baraffe, I., Homeier, D., Allard, F., & Chabrier, G. 2015, A&A, 577, A42
Baron, F., Artigau, É., Rameau, J., et al. 2018, AJ, 156, 137
Bell, C. P. M., Mamajek, E. E., & Naylor, T. 2016, in IAU Symp. 314, Young Stars & Planets Near the Sun, ed. J. H. Kastner et al. (Cambridge: Cambridge Univ. Press), 41
Berger, J. O., Bernardo, J. M., & Sun, D. 2009, arXiv:0904.0156
Biller, B. A., Close, L. M., Masciadri, E., et al. 2007, ApJS, 173, 143
Biller, B. A., Liu, M. C., Wahhaj, Z., et al. 2013, ApJ, 777, 160
Blunt, S., Nielsen, E. L., Rosa, D., et al. 2017, AJ, 153, 229
Bowler, B. P. 2016, PASP, 128, 102001
Bowler, B. P., Liu, M. C., Shkolnik, E. L., & Dupuy, T. J. 2013, ApJ, 774, 55
Bowler, B. P., Liu, M. C., Shkolnik, E. L., & Tamura, M. 2015, ApJS, 216, 7
Brandt, T. D., McElwain, M. W., Turner, E. L., et al. 2014, ApJ, 794, 159
Cassan, A., Kubas, D., Beaulieu, J.-P., et al. 2012, Natur, 481, 167
Chabrier, G., Baraffe, I., Allard, F., & Hauschildt, P. H. 2005, arXiv:astro-ph/0509798
Chauvin, G., Lagrange, A.-M., Bonavita, M., et al. 2010, A&A, 509, A52
Chauvin, G., Lagrange, A.-M., Dumas, C., et al. 2004, A&A, 425, L29
Chauvin, G., Lagrange, A.-M., Zuckerman, B., et al. 2005, A&A, 438, L29
Chauvin, G., Vigan, A., Bonnefoy, M., et al. 2015, A&A, 573, A127
Cumming, A., Butler, R. P., Marcy, G. W., et al. 2008, PASP, 120, 531
David, T. J., & Hillenbrand, L. A. 2015, ApJ, 804, 146
de la Reza, R., Torres, C. A. O., Quast, G., Castilho, B. V., & Vieira, G. L. 1989, ApJL, 343, L61
Deacon, N. R., Schlieder, J. E., & Murphy, S. J. 2016, MNRAS, 457, 3191
Delorme, P., Gagné, J., Girard, J. H., et al. 2013b, A&A, 553, L5
Delorme, P., Gagné, J., Lannier, J., Lagrange, A. M., & Chauvin, G. 2013a, MmSAI, 84, 1013
Dong, S., & Zhu, Z. 2013, ApJ, 778, 53
Duchêne, G., & Kraus, A. 2013, ARA&A, 51, 269
Dupuy, T. J., Liu, M. C., Allers, K. N., et al. 2018, AJ, 156, 57
Durkan, S., Janson, M., & Carson, J. C. 2016, ApJ, 824, 58
Eisenbeiss, T., Ammler-von Eiff, M., Roell, T., et al. 2013, A&A, 556, A53
Fernandes, R. B., Mulders, G. D., Pascucci, I., Mordasini, C., & Emsenhuber, A. 2019, ApJ, 874, 81
Fontanive, C., Biller, B., Bonavita, M., & Allers, K. 2018, MNRAS, 479, 2702
Foreman-Mackey, D., Hogg, D. W., Lang, D., & Goodman, J. 2013, PASP, 125, 306
Forgan, D., & Rice, K. 2013, MNRAS, 432, 3168
Fortney, J. J., Marley, M. S., Saumon, D., & Lodders, K. 2008, ApJ, 683, 1104
Gagné, J., Mamajek, E. E., Malo, L., et al. 2018, ApJ, 856, 23
Gaia Collaboration, Brown, A. G. A., Vallenari, A., et al. 2018, A&A, 616, A1
Galicher, R., Marois, C., Macintosh, B., et al. 2016, A&A, 594, A63
Gauza, B., Béjar, V. J. S., Pérez-Garrido, A., et al. 2015, ApJ, 804, 96
Goldman, B., Marsat, S., Henning, T., Clemens, C., & Greiner, J. 2010, MNRAS, 405, 1140
Goodman, J., & Weare, J. 2010, CAMCOS, 5, 65
Heinze, A. N., Hinz, P. M., Kenworthy, M., et al. 2010a, ApJ, 714, 1570
Heinze, A. N., Hinz, P. M., Sivanandam, S., et al. 2010b, ApJ, 714, 1551
Howard, A. W., Marcy, G. W., Johnson, J. A., et al. 2010, Sci, 330, 653
Ireland, M. J., Kraus, A., Martinache, F., Law, N., & Hillenbrand, L. A. 2011, ApJ, 726, 113
Itoh, Y., Hayashi, M., Tamura, M., et al. 2005, ApJ, 620, 984
Janson, M., Bonavita, M., Klahr, H., et al. 2011, ApJ, 736, 89
Johnson, J. A., Aller, K. M., Howard, A. W., & Crepp, J. R. 2010, PASP, 122, 905
Kasper, M., Apai, D., Janson, M., & Brandner, W. 2007, A&A, 472, 321
Kastner, J. H., Zuckerman, B., Weintraub, D. A., & Forveille, T. 1997, Sci, 277, 67
Kipping, D. M. 2013, MNRAS, 434, L51
Kraus, A. L., Ireland, M. J., Cieza, L. A., et al. 2014, ApJ, 781, 20
Lachapelle, F.-R., Lafrenière, D., Gagné, J., et al. 2015, ApJ, 802, 61
Lafrenière, D., Doyon, R., Marois, C., et al. 2007, ApJ, 670, 1367
Lafrenière, D., Jayawardhana, R., & van Kerkwijk, M. H. 2008, ApJL, 689, L153
Lafrenière, D., Jayawardhana, R., & van Kerkwijk, M. H. 2010, ApJ, 719, 497
Lafrenière, D., Jayawardhana, R., van Kerkwijk, M. H., Brandeker, A., & Janson, M. 2014, ApJ, 785, 47
Lagrange, A.-M., Gratadour, D., Chauvin, G., et al. 2009, A&A, 493, L21
Lannier, J., Delorme, P., Lagrange, A. M., et al. 2016, A&A, 596, A83
Lindegren, L., Hernandez, J., Bombrun, A., et al. 2018, A&A, 616, A2
Luhman, K. L., Mamajek, E. E., Allen, P. R., Muench, A. A., & Finkbeiner, D. P. 2009, ApJ, 691, 1265
Luhman, K. L., Wilson, J. C., Brandner, W., et al. 2006, ApJ, 649, 894
Macintosh, B., Graham, J. R., Barman, T., et al. 2015, Sci, 350, 64
Makarov, V. V., & Urban, S. 2000, MNRAS, 317, 289
Mamajek, E. E. 2016, in IAU Symp. 314, Young Stars & Planets Near the Sun, ed. J. H. Kastner (Cambridge: Cambridge Univ. Press), 21
Marois, C., Macintosh, B., Barman, T., et al. 2008, Sci, 322, 1348
Marois, C., Zuckerman, B., Konopacky, Q. M., Macintosh, B., & Barman, T. 2010, Natur, 468, 1080
Masciadri, E., Mundt, R., Henning, T., Alvarez, C., & Barrado y Navascués, D 2005, ApJ, 625, 1004
Mayor, M., Marmier, M., Lovis, C., et al. 2011, arXiv:1109.2497
Meshkat, T., Bailey, V. P., Su, K. Y. L., et al. 2015a, ApJ, 800, 5
Meshkat, T., Kenworthy, M. A., Reggiani, M., et al. 2015b, MNRAS, 453, 2533
Meshkat, T., Mawet, D., Bryan, M. L., et al. 2017, AJ, 154, 245
Metchev, S. A., & Hillenbrand, L. A. 2009, ApJS, 181, 62
Meyer, M. R., Amara, A., Reggiani, M., & Quanz, S. P. 2018, A&A, 612, L3
Millar-Blanchaer, M. A., Graham, J. R., Pueyo, L., et al. 2015, ApJ, 811, 18
Murphy, S. J., & Lawson, W. A. 2015, MNRAS, 447, 1267
Murphy, S. J., Lawson, W. A., & Bessell, M. S. 2013, MNRAS, 435, 1325
Naud, M.-E., Artigau, É., Doyon, R., et al. 2017, AJ, 154, 129
Naud, M.-E., Artigau, É., Malo, L., et al. 2014, ApJ, 787, 5
Nielsen, E. L., Liu, M. C., Wahhaj, Z., et al. 2013, ApJ, 776, 4
Pecaut, M. J., & Mamajek, E. E. 2016, MNRAS, 461, 794
Raghavan, D., McAlister, H. A., Henry, T. J., et al. 2010, ApJS, 190, 1
Rameau, J., Chauvin, G., Lagrange, A.-M., et al. 2013a, ApJL, 772, L15
Rameau, J., Chauvin, G., Lagrange, A.-M., et al. 2013b, A&A, 553, A60
Rebolo, R., Zapatero Osorio, M. R., Madruga, S., et al. 1998, Sci, 282, 1309
Reggiani, M., Meyer, M. R., Chauvin, G., et al. 2016, A&A, 586, A147
Reid, I. N., & Walkowicz, L. M. 2006, PASP, 118, 671
Sahlmann, J., Segransan, D., Queloz, D., & Udry, S. 2011, in IAU Symp. 276, The Astrophysics of Planetary Systems: Formation, Structure, and Dynamical Evolution, ed. A. Sozzetti (Cambridge: Cambridge Univ. Press), 117
Santos, N. C., Adibekyan, V., Figueira, P., et al. 2017, A&A, 603, A30
Schaller, G., Schaerer, D., Meynet, G., & Maeder, A. 1992, A&A, 96, 269
Shkolnik, E. L., Allers, K. N., Kraus, A. L., Liu, M. C., & Flagg, L. 2017, AJ, 154, 69
Siess, L., Dufour, E., & Forestini, M. 2000, A&A, 358, 593
Snellen, I. a. G., & Brown, A. G. A. 2018, NatAs, 2, 883
Stone, J. M., Skemer, A. J., Hinz, P. M., et al. 2018, AJ, 156, 286
Tabachnik, S., & Tremaine, S. 2002, MNRAS, 335, 151
Todorov, K., Luhman, K. L., & McLeod, K. K. 2010, ApJL, 714, L84
Torres, C. A. O., da Silva, L., Quast, G. R., de la Reza, R., & Jilinski, E. 2000, AJ, 120, 1410
Torres, C. A. O., Quast, G. R., Melo, C. H. F., & Sterzik, M. F. 2008, in Handbook of Star-forming Regions, Volume II, ed. B. Reipurth (San Francisco, CA: ASP), 757
Uyama, T., Hashimoto, J., Kuzuhara, M., et al. 2017, AJ, 153, 106
Vigan, A., Bonavita, M., Biller, B., et al. 2017, A&A, 603, A3
Vigan, A., Patience, J., Marois, C., et al. 2012, A&A, 544, A9
Wahhaj, Z., Liu, M. C., Nielsen, E. L., et al. 2013, ApJ, 773, 179
Wang, J. J., Graham, J. R., Dawson, R., et al. 2018, AJ, 156, 192
Zuckerman, B. 2019, ApJ, 870, 27
Zuckerman, B., Bessell, M. S., Song, I., & Kim, S. 2006, ApJL, 649, L115
Zuckerman, B., Rhee, J. H., Song, I., & Bessell, M. S. 2011, ApJ, 732, 61
Zuckerman, B., Song, I., & Bessell, M. S. 2004, ApJL, 613, L65
Zuckerman, B., Song, I., Bessell, M. S., & Webb, R. A. 2001a, ApJL, 562, L87
Zuckerman, B., Song, I., & Webb, R. A. 2001b, ApJ, 559, 388